JOINT EUROPEAN TORUS JET

JET–P(91)31

M.J. Alava, J.A. Heikkinen
and JET Team

A Parameter Study of Mode Conversion at Ion-Ion Hybrid Resonances for ICRF-Heating Schemes in JET

A Parameter Study of Mode Conversion at Ion-Ion Hybrid Resonances for ICRF-Heating Schemes in JET

M.J. Alava, J.A. Heikkinen[1]
and JET Team*

JET-Joint Undertaking, Culham Science Centre, OX14 3DB, Abingdon, UK

[1]Nuclear Enguineering Laboratory, Tekniikant. 4, PO Box 208, SF-02150 Espoo, Finland
** See Appendix 1*

Preprint of Paper to be submitted for publication in
Physica Scripta

ABSTRACT.

By solving the wave equation for the radial electric field locally around the resonance layer of the fast Alfven wave, some complex characteristics of mode conversion physics can be elucidated and analyzed in the ion cyclotron range of frequencies. The validity of the Budden and tunnelling model for the conversion studies is explored, and the conversion coefficient for the ion-ion hybrid resonance in the presence of cyclotron damping is found in closed form. The analytical results are compared with the numerical solution of the full wave equations expanded to second order in ion Larmor radius. It is found that the standard tunnelling solutions can be erroneous, not only in the case of strong damping, but also when the linearization of the plasma parameters around the resonance, peculiar to the tunnelling model, becomes inaccurate. The effects of the damping and cavity resonances on the conversion are separated in the derived analytical estimates, and the limits of the local theory of conversion are determined.

Contents

1 Introduction

The recent success of ion cyclotron resonance heating (ICRH) has stimulated interest in detailed theoretical models for calculating the wave absorption for relevant heating scenarios. A number of numerical codes have been developed to solve the global energy-conserving wave equations inside the tokamak chamber. While the codes written in a slab geometry [1-5] have confirmed most predictions of the analytical theory of absorption mechanisms, the two-dimensional codes [6-8] including the poloidal and radial variation have been of great value in resolving the wave field spatially and finding the effects of cavity resonances and the poloidal field on coupling resistance and absorption.

According to the analytical theory, the fast wave power is absorbed by ions at the cyclotron resonance or by electrons via Landau or Transit Time damping. The cyclotron damping is also accompanied by mode conversion [9] which, at the plasma center, converts the fast wave power to that of ion Bernstein waves. In many heating scenarios the latter mechanism may be as important as the cyclotron absorption. This follows because the cyclotron absorption becomes weaker, and mode conversion stronger, for smaller parallel wavenumbers for which the antenna coupling is more effective. The absorption of the converted wave power is not well understood because of the complex propagation of the ion Bernstein waves in a toroidal geometry. In particular, the relative amount of the absorption to ions and electrons, respectively, is poorly known.

The mode conversion process [10] can take place in an inhomogeneous plasma where two different wave branches have a similar dispersion at a particular spatial location. This causes the incident wave energy flux to split into the fluxes of various emanating wave modes. Fig. 1 shows a typical sketch of the spatial variation of the wavenumber based on dispersion relations at local parameters. Far from the resonance the wave branches propagate independently, while near the resonance the dispersion characteristics get mixed.

For simplified cases it is possible to derive relations between the incident, converted, transmitted and reflected wave energy fluxes [11]. Assuming a second-order model equation (Budden equation)

$$\lambda^2 x E'' + (\lambda^2 x + \gamma) E = 0 \tag{1}$$

for the time-independent wave equation, the amplitude coefficients of reflection (R) and transmission (T) (i.e tunnelling) read

$$| R | = 1 - \exp(-2\eta), \qquad | T | = \exp(-\eta) \tag{2}$$

for the right going wave, and

$$| R | = 0, \qquad | T | = \exp(-\eta) \tag{3}$$

for the left going wave. Here $\eta = \mid \pi\gamma/2\lambda^2 \mid$ and x is the spatial coordinate. The prime denotes the derivative with respect to x. γ is a complex constant while λ^2 is a positive number. To obtain the results in Eqs.(2) and (3), asymptotic solutions of Eq.(1) at large $\mid x \mid$ have been matched to the local solution at small $\mid x \mid$. In both cases $\mid R \mid^2 + \mid T \mid^2 < 1$, indicating absorption at the singularity $x = 0$. An analysis of a higher order tunnelling equation [12,13]

$$E'''' + \lambda^2 x E'' + \alpha\lambda^2 E' + (\lambda^2 x + \gamma)E = 0, \tag{4}$$

where α is a complex constant, gives the same reflection and transmission coefficients, but here the absorbed fraction of the wave power $1 - \mid R \mid^2 - \mid T \mid^2$ equals the conversion coefficient into the short wavelength wave mode which appears in the solution of Eq.(4). In the present case η is given by $\eta = \mid (\pi/2)(1+\gamma)/\lambda^2 \mid$.

Eqs.(1) or (4) are often used for estimating the conversion at ion-ion hybrid and harmonic resonances at the plasma center. In the case of weak damping around the resonance, the wave equations can be put into the form of Eqs.(1) or (4) with linear coefficients, often to a good accuracy, if weak gradients at the plasma centre make the equations valid for a sufficiently large region around the resonance. There are several papers [2,3,5,14], in which the reflection, transmission and conversion coefficients are calculated for a large range of parameters by solving numerically the wave equations around the resonance. On the other hand, only few comparative studies of the Budden results, Eqs. (2) and (3), and numerical solutions have appeared. By taking the WKB limit [15] in considering the mode conversion process, Weynants [16] has been able to include the corrections to Eqs. (2) and (3) due to the damping decrements of the fast and slow waves and has found a good agreement between the corrected formulas and all the published results given in Refs. [2] and [3]. The numerical results show that the transmission is fairly well given by $\mid T \mid = e^{-\eta}$. The reflection coefficient from the high magnetic field side remains zero, while the other reflection coefficient and the conversion coefficients have the general form [17]

$$\mid R \mid^2 = (1 - e^{-2\eta})^2 e^{-2\alpha_{RL}\kappa_D^2}$$

$$\mid C \mid^2 = (1 - e^{-2\eta}) e^{-2\eta} e^{-2\alpha_{CL}\kappa_D^2} \tag{5}$$

for the low field incidence, and

$$\mid C \mid^2 = (1 - e^{-2\eta})^2 e^{-2\alpha_{CH}\kappa_D^2} \tag{6}$$

for the high field incidence, where for each case the function α depends on η and plasma parameters, and κ_D is a function proportional to the Doppler- width of the cyclotron resonance. κ_D can be found analytically for each case, but only empirical formulae, determined from the numerical analysis, exist for α, the general behaviour of which is unpublished. In the method used by Weynants, the damping corrections are found analytically by following each wave inside the evanescent region around the resonance and

by evaluating the damping decrements from the integrals of $\mathrm{Im}\{k_\perp\}$ along the path. In these studies, the wavenumbers $k_\perp$ for each mode are determined from the WKB approximation of the dispersion relation. The good agreement with the numerical results in this method for ion-ion hybrid resonances, as well as for cyclotron harmonics, emphasizes the very simple nature of the mode conversion physics. However, the damping corrections obtained by the WKB method are, in general, difficult to calculate; one has to solve the dispersion relation for each branch wavenumber, find the right paths and make the integrations. Furthermore, this method as well as the others do not definitely state when they are valid and when not.

Recently, a more rigorous theory of the interplay between the mode conversion and cyclotron absorption was developed by Chow *et al.* [18], who consider the mode conversion in the Budden formalism keeping the cyclotron damping as a small perturbation. The damping corrections obtained by them show a good agreement with numerical solutions, provided the Budden resonance and the ion cyclotron resonance are well separated. With this method it is not possible to separate the converted power from the damped power so that only the reflection and transmission coefficients can be obtained analytically. In an earlier work by Swanson [19], the conversion coefficient was calculated using the Green's function approach. This method leads to an integral equation which can be solved numerically by iterative methods. In that work it was possible to study the effect of localized absorption on the mode conversion. A remarkable reduction in the numerical effort was achieved by Kay *et al.* [20], who solve a second order mode conversion equation, by taking advantage of the localised nature of the slow mode and treating it as a driven response to the fast Alfvén wave. This equation is integrated numerically, and the results agree well with those obtained using higher-order equations. The effect of damping on the conversion was studied for the case of harmonic heating of deuterium and D(H) minority heating. The models of Swanson and Kay *et al.* do not give analytically derived estimates for the effect of damping. Moreover, the validity limits of these models are not studied in detail.

In the present work we do a local analysis of the mode conversion process to study the validity of the Budden formalism. By inspecting the wave equation for the radial electric field (E_x) near the ion-ion hybrid resonance, we are able to express the converted power as a function of the local poloidal electric field (E_y) and plasma parameters. The validity of this estimate and its relation to the Budden coefficients in Eqs. (2) and (3) are explored. The effect of cyclotron damping is analysed in the same context, and the corresponding analytical correction to the conversion coefficient is found. A systematic comparison of the analytical results with the numerical solution of the full wave equations is presented for three relevant minority heating scenarios; D(H), D(^{3}He), and T(D) ion cyclotron heating with JET like parameters.

In Section. 2 we present our local theory of the mode conversion process. Section. 3 is devoted to the description and the results of the numerical method and to the comparison with the analytical estimates. Finally, in Section 4 we present our conclusions and discuss the validity of the Budden formalism in real experiments.

2 Local theory of mode conversion for ion-ion hybrid resonances

2.1 Basic equations and the connection to the tunnelling equation

In the case of the ion-ion hybrid resonance, we write the wave equations for the radial (E_x) and poloidal (E_y) electric fields in a simplified form

$$\sigma E_x'' + (S - n_z^2)E_x - iDE_y = 0 \tag{7}$$

$$E_y'' + (S - n_z^2)E_y + iDE_x = 0, \tag{8}$$

where the dielectric tensor elements are given by

$$S = 1 + \sum_i \kappa_i [Z(a_{1i}) + Z(a_{-1i})] \tag{9}$$

$$D = -\sum_i \kappa_i [Z(a_{1i}) - Z(a_{-1i})] - \frac{\omega_{pe}^2}{\Omega_e \omega} \tag{10}$$

$$\lambda_n = -\sum_i \kappa_i r_i^2 Z(a_{ni}) \tag{11}$$

with $\sigma_n = (\lambda_{-n} + \lambda_n)/2$ and $\sigma = \sigma_2 - \sigma_1$. We have defined $\kappa_i = \omega_{pi}^2 c/(2\omega^2 n_z v_{Ti})$, $a_{ji} = (1 - j\Omega_i/\omega)/(n_z v_{Ti}/c)$ and $a_{0e} = c/n_z v_{Te}$. Z denotes the complex-valued plasma dispersion function, and summation extends over all ion species. v_{Ti}, ω_{pi} and Ω_i are the thermal velocity, plasma frequency and cyclotron frequency, respectively, of the i-th species (i=e, for electrons), c is the speed of the light and ω is the angular frequency of the radiation. All the lengths are normalised to c/ω. r_i denotes the ion Larmor radius $(v_{Ti}/\sqrt{2}c)(\omega/\Omega_i)$. In Eqs. (7) and (8) the prime denotes the derivative with respect to x, the radial coordinate. We have neglected magnetic shear and toroidicity and write the equations in a plane stratified limit. n_z denotes the wave refractive index in the direction of the magnetic field. The corresponding index, n_y, in the poloidal direction is taken to be zero. We note that σ gives the kinetic correction to second order in ion Larmor radius, and electron inertia effects are neglected, i.e E_z is assumed to be small for each wave branch. The latter approximation is often valid at the high density plasma at the plasma centre. We have neglected various kinetic corrections as well as a number of terms arising from the gradients of the background plasma parameters [1-7]. The numerous assumptions in

obtaining Eqs. (7) and (8) are inspected in the numerical study of the more complete equations (28)-(30), to be presented in the next Section.

Using the WKB approximation $E' = in_\perp E$ and Fourier analyzing Eqs. (7) and (8) gives a dispersion relation

$$n_\perp^4 + An_\perp^2 + B = 0, \tag{12}$$

where $A = (n_z^2 - S)/\sigma + 2(n_z^2 - S - D)$, $B = [(S - n_z^2)^2 - D^2]/\sigma$ and $n_\perp$ denotes the perpendicular component of the refractive index. The resonance is obtained at $A = 0$. By linearizing A and B around the resonance (at $x = 0$) and using the inverse transform $in_\perp E = E'$, Eq. (12) yields the tunnelling equation (4) with $\alpha = 0$, $\lambda^2 = -A'(-B'/A')^{-3/2}$ and $\gamma = B(-B'/A')^{-2}$. Note that B and the derivatives B' and A' are calculated at $x = 0$. It has been shown for experimental parameters [21] that the roots of the dispersion relation obtained by linearizing A and B in Eq. (12) can well match the roots of Eq.(12) around the resonance including the region from the resonance at $A = 0$ to the cut-off at $B = 0$. It is obvious from the asymptotic analysis of the tunnelling equation that the linearization has to be done accurately near the resonance to obtain the correct conversion coefficient, but it is not clear how well and how far from the resonance the linearized dispersion relation has to match the true dispersion behaviour. We note that the asymptotic analysis of Eq. (4) leading to the expressions in Eqs. (2) and (3) is valid provided $\lambda^2 > -1$, i.e A and B have to be real-valued, at least.

Far from the resonance, the roots of Eq.(12) are well separated and can be approximated by

$$n_{\perp f}^2 = \frac{(S - n_z^2)^2 - D^2}{S - n_z^2} \tag{13}$$

$$n_{\perp B}^2 = \frac{S - n_z^2}{\sigma}. \tag{14}$$

Near the resonance at $\mathrm{Re}\{S\} = n_z^2$ the roots coalesce and form a complex-conjugate pair as is shown in Fig.1. This is true even for real S, D and σ. We note that $|\sigma| \ll |S|, |D|$ so that the ion Bernstein wavenumber $n_{\perp B}$ is in general much larger than that of the fast wave, $n_{\perp f}$, far from the resonance.

Fig. 2 shows S, D and σ around the resonance for D(^{3}He) minority heating scenario in the JET-plasma. We have chosen $N = 5 \times 10^{19}\mathrm{m}^{-3}$ for the electron density, $T = 5$ keV for the temperature and $n_z = 4$. In this case S, D and σ are clearly complex in the region from the cyclotron resonance up to the ^{3}He-D hybrid resonance which makes the asymptotic analysis of Eq. (4) questionable in the present case.

2.2 Conversion coefficient and solution for E_x

Solving Eqs. (7) and (8) for general S, D and σ by analytical means is clearly hopeless. Noting the long wavelength of the incident fast wave we make an assumption that DE_y/σ is constant around the resonance. In this case Eq. (7) becomes

$$E_x'' + f(x)E_x = g, \tag{15}$$

where $f(x) = (S - n_z^2)/\sigma$ and $g = iD(0)E_y(0)/\sigma(0)$. Expanding $f(x)$ around the resonance at $x = 0$

$$f(x) = (f_r' + if_i')x + f_i, \tag{16}$$

where f_r and f_i denote the real and imaginary parts of f evaluated at $x = 0$, one can put Eq.(15) into the form

$$E_x'' + sE_x = g(f_r' + if_i')^{-2/3}, \tag{17}$$

where the substitution

$$s = (f_r' + if_i')^{1/3}x + i(f_r' + if_i')^{-2/3}f_i \tag{18}$$

is made and the prime indicates the derivative with respect to the new variable s. Eq. (17) can be solved in terms of the Airy functions. To obtain meaningful asymptotic solutions we model $f(x)$ with a bilinear curve, as shown in Fig. 3. We assume $\sigma = \sigma(0)$, and consider the spatial variation of S only. $f(x)$ is described by Eq.(16) for $x < -f_i/f_i'$ (region I) while $f(x) = f_r'x$ for $x > -f_i/f_i'$ (region II). This model accounts for the increase of f_i from $x = 0$ towards the cyclotron resonance and for the attenuation of f_i as $x \to \infty$. Note that we underestimate the damping in the neighbourhood of the confluence, while the damping at $x = 0$ is correctly described. Note also that we have assumed f_r' and f_i' to be positive at the resonance.

The solutions of Eq.(17) can be written as

$$I \qquad E_x = -\pi g a_1^2[Gi(-s) + R_a Ai(-s)] \tag{19}$$

$$II \qquad E_x = -\pi g a_2^2\{Gi(-s) - iAi(-s) + C_a[Bi(-s) - iAi(-s)]\} \tag{20}$$

in the regions I and II, respectively. We have defined $a_1 = (f_r' + if_i')^{-1/3}$, $a_2 = (f_r')^{-1/3}$ and s is defined by Eq. (18), separately for each region. R_a and C_a are the integration constants to be determined from the condition that E_x and E_x' are continuous at $x = -f_i/f_i'$. Note that E_x vanishes at $x = -\infty$ and describes an oscillatory backward propagating wave for large positive x. From the matching conditions we find

$$C_a = \frac{-Ai_1'(Gi_2 - iAi_2) + \frac{a_1}{a_2}Ai_1(Gi_2' - iAi_2') + \frac{a_1^2}{a_2^2}(Gi_1Ai_1' - Gi_1'Ai_1)}{Ai_1'(Bi_2 - iAi_2) - \frac{a_1}{a_2}Ai_1(Bi_2' - iAi_2')}, \tag{21}$$

where we have defined $Ai_1 = Ai(-s_1)$, $Ai_2 = Ai(-s_2)$ with s_1 and s_2 denoting the limit values of s at $x = -f_i/f_i'$;

$$s_1 = -\frac{f_i f_r'/f_i'}{(f_r' + if_i')a_1} \tag{22}$$

in the region I, and

$$s_2 = -\frac{f_i/f_i'}{a_2} \tag{23}$$

in the region II. The primes in the Airy functions in Eq. (21) indicate the derivatives with respect to the argument of the function.

We are now able to calculate the kinetic power flux I_k =Im$(\sigma E_x^* E_x')$, which also gives us the converted power flux in the mode conversion. A simple calculation of I_k for large positive x gives

$$I_{k\infty} = -\pi \frac{\mid D(0) \mid^2}{S_r'} \mid E_y(0) \mid^2 \mid 1 + C_a \mid^2, \tag{24}$$

where S_r' denotes the derivative of the real part of S at the resonance. In the case of no damping, $f_i = 0$, $a_1 = a_2$ and $s_1 = s_2 = 0$. This gives $C_a = 0$, and Eq. (24) reduces to Eq. (7) in Ref. [22] derived for the converted power flux with real S and σ. With large $\mid f_i/f_i' \mid$, s_1 and s_2 become large and the asymptotic value of C_a approaches -1. In this limit the converted power appears to vanish according to Eq. (24). We therefore conclude that the term $\mid 1 + C_a \mid^2$ gives the effect of the ion cyclotron damping of the ion Bernstein wave on the conversion, and the radial field of the converted wave is correspondingly described by Eqs. (19) and (20). $E_y(0)$ is, of course, unknown and is determined by Eq. (8).

Neglecting $\sigma E_x''$ in Eq. (7), one finds from Eqs. (7) and (8)

$$E_y'' + \frac{(S - n_z^2)^2 - D^2}{S - n_z^2} E_y = 0. \tag{25}$$

This equation describes well the long wavelength fast wave and, in the absence of damping, can be transformed into the form of Eq. (1). Making the linearizations $S - n_z^2 = S'x$ and $D^2 = D_0^2 + (D^2)'x$ we find Eq. (1) with $\eta = -(\pi/2)(D_0^2/S')/[-(D^2)'/S']^{1/2}$. It is not difficult to find from the analysis of Eq. (1) that the ratio of $\mid E_y(0) \mid^2$ to the incident power flux I_i is given by [23]

$$\frac{\mid E_y(0) \mid^2}{I_i} = \frac{e^{-2\eta}(1 - e^{-2\eta})}{2\eta n_f}, \tag{26}$$

where $n_f = [-(D^2)'/S']^{1/2}$. Substituting $\mid E_y(0) \mid$ from Eq. (26) to Eq. (24) gives $I_k/I_i = e^{-2\eta}(1 - e^{-2\eta})$ for the converted power fraction in the case of no damping. This is consistent with the Budden result for the absorbed power. In fact, direct integration of the derivative of the Poynting flux of the fast wave $I_f = \mathrm{Im}(E_y^* E_y')$ over the resonance gives the same result as Eq. (24) with $C_a = 0$ [22].

Supported by the fact that the converted wave is damped more strongly than the fast wave around the resonance and that the evanescence of the fast wave dominates over its attenuation in interesting cases where the converted wave is not completely damped, we postulate the approximation

$$I_k/I_i \approx e^{-2\eta}(1 - e^{-2\eta}) \mid 1 + C_a \mid^2 \tag{27}$$

for the converted power fraction. I_i denotes the incident power flux towards the resonance calculated at the cut-off. Since the cyclotron damping of the converted wave is accounted for by the term $\mid 1 + C_a \mid^2$, Eqs. (24) and (27) obviously give that fraction of the converted power which will be damped by other mechanisms like electron damping.

2.3 Validity of the analytical estimates

In the conversion analysis presented in this Section we have been able to identify in the conversion physics three relatively independent mechanisms. The first one is the growth of the electric field of the converted wave which is driven by a local value of the poloidal component of the fast wave electric field. The second one is the cyclotron damping of the converted wave which counteracts the fast wave drive. The asymptotic result in Eq. (24) which accounts for these two mechanisms is valid provided the linearizations and the assumption of constant E_y (and constant D and σ) are good approximations over the region $\mid x \mid < L$, where we demand $L > \mid a_1 \mid, a_2$.

$\mid a_1 \mid$ and a_2 are usually of the same order of magnitude, and are about 0.005 in the case of Figs. 2 and 3. At the plasma edge these are much shorter due to the lower temperature

and steeper gradients. The basic mechanism of the conversion is, therefore, limited to a very short region around the resonance, defined by $\mid a_1 \mid$ and a_2. The damping of the converted wave may take place over a longer distance, if $\mid f_i/f_i' \mid$ much exceeds a_2. In this case it may often be necessary to solve Eq. (15) numerically to account for a particular form of f_i (e.g. a Gaussian for a Maxwellian distribution).

The local value of E_y at the resonance is not so much affected by the conversion itself but is determined by a number of external conditions like the length of the evanescent region in front of the resonance, damping, wall reflection and cavity resonance formation in a real tokamak chamber geometry. In the analysis of the conversion at the edge plasma [22,24], Eq. (24) was found useful because $\mid E_y \mid$ at the edge resonances is strongly affected by the boundary conditions at the wall or antenna, and in most cases is easy to calculate as a function of the incident power flux. At the resonances in the plasma centre, the value of $\mid E_y \mid$ should be mainly affected by the length of the evanescent region but may in some cases be strongly influenced by the other effects listed above. The scale length for the variation of $\mid E_y \mid$ is clearly much longer than $\mid a_{1,2} \mid$ which separates the third mechanism, the effects affecting on $\mid E_y \mid$, from the other two.

3 Comparison of analytical theory with numerical results

3.1 Basic equations and the numerical method

In this Section, we test the physics described in the last Section by solving the more advanced wave equations [1-7] which include the effects of the gradients in the plasma parameters, finite ion Larmor radius and electron inertia. We assume a plane-stratified model and write the equations

$$(\sigma E_x')' - i(\delta E_y')' + (S - n_y^2(1+\rho) - n_z^2)E_x - in_y E_y' \\ -i(D - \delta n_y^2)E_y - in_z E_z' = 0 \tag{28}$$

$$i(\delta E_x')' + (\rho E_y')' + i(D - \delta n_y^2)E_x - in_y E_x' + E_y'' \\ +(S - n_z^2 - \sigma n_y^2)E_y + n_y n_z E_z - n_z(\xi E_z)' = 0 \tag{29}$$

$$-in_z E_x' + n_y n_z E_y + n_z \xi E_y' + E_z'' + (P - n_y^2)E_z = 0, \tag{30}$$

where E_x, E_y and E_z denote the electric field components perpendicular to the magnetic field (x,y) and along it (z), respectively. A plasma slab inhomogeneous in the radial direction (x) is assumed. The terms proportional to σ, $\delta = \delta_2 - 2\delta_1$ and $\rho = 2\lambda_0 - 3\sigma_1 + \sigma_2$ with $\delta_n = (\lambda_{-n} - \lambda_n)/2$ give the finite ion Larmor radius corrections. The Transit Time damping is introduced by the terms proportional to $\xi = \xi_0 - (\xi_1 + \xi_{-1})/2$ with $\xi_n = \sum_i \kappa_i r_i^2 a_{0i} Z'(a_{ni})$. The last equation (30) accounts for the electron inertia effects with finite

$$P = 1 - (\frac{\omega_{pe}^2}{\omega^2})a_{0e}^2 Z'(a_{0e}). \tag{31}$$

Assuming that $\mid \sigma \mid, \mid \delta \mid, \mid \rho \mid \ll 1$ hold, we have neglected a few terms proportional to the second derivatives of σ_1 and δ_1 and to the products of in_y and the kinetic terms. We note that Eqs. (28)-(30) are still energy conserving [4]. Some kinetic corrections proportional to E_z are also neglected [7].

Eqs. (28)-(30) in a reduced form or even in a more complete form have been solved numerically by a number of authors for a variety of cases. The popular approach has been the use of finite elements to discretize the equations and the implementation of global boundary conditions to include a maximum amount of physics. In the present work our interest is in the local behaviour of the solution around the resonance. To make the integration length short and to simplify the physics, we only look for a solution near the resonance. A widely used method [2,3,5,14,24] is to decompose the total field at the boundaries into the wave branches obtained by a WKB analysis of Eqs. (28)-(30). The total field includes the incident fast wave branch, the corresponding energy flux of which is normalized to unity, the reflected and transmitted fast wave branches and the converted and evanescent slow wave branches. The details of the numerical method are presented in Ref. [24] and will not be presented here.

3.2 Numerical analysis

Solving Eqs. (28)-(30) with a cubic finite element method and using the wave decomposition at the boundaries, we can calculate the conversion, reflection and transmission coefficients for an incoming fast wave with sufficient accuracy and with reasonable computing time for routine runs. The energy flux of the i-th mode is given by

$$I_{xi} = \mid \tau_i \mid^2 \{\mathrm{Re}(\mathrm{E_{yi}^* B_{zi}} - \mathrm{E_{zi}^* B_{yi}}) + \mathrm{Im}[\mathrm{E_{xi}^*}(\sigma \mathrm{E'_{xi}} - \mathrm{i}\delta \mathrm{E'_{yi}}) + \mathrm{E_{yi}^*}(\mathrm{i}\delta \mathrm{E'_{xi}} + \rho \mathrm{E'_{yi}})]\}, \tag{32}$$

where τ_i denotes the amplitude of the i-th mode, $B_{zi} = -iE'_{yi} - n_y E_{xi}$ and $B_{yi} = n_z E_{xi} + iE'_{zi}$, and E_{xi}, E_{yi} and E_{zi} are the components of the polarization vector $\vec{E}_i$ of the i-th mode. The latter term in Eq.(32) represents the kinetic power flux and the former one is the usual Poynting flux. We define

$$\mid C \mid^2 = \frac{I_{xB}(L)}{I_{xf}(0)} \tag{33}$$

for the conversion coefficient, where $x = 0, L$ define the left and right boundary, correspondingly, and the indices $i = f, f_-$ denote the rightgoing and leftgoing fast wave, respectively. The definition in Eq. (33) allows only the low field incidence but includes

the conversion of the fast wave reflected from the outside of the calculation region. We have $\mid R \mid^2 = -I_{xf-}(0)/I_{xf}(0)$ for the reflection coefficient at the left boundary and $\mid T \mid^2 = I_{xf}(L)/I_{xf}(0)$ for the transmission coefficient at the right boundary, for the low field incidence.

To solve Eqs. (28)-(30) across the resonance, we have chosen model profiles for the density, temperature and the magnetic field near the resonance with JET-like parameters. For the magnetic field we have $B = B_0/(1 - x/R_0)$, where B_0 denotes the magnetic field at the major radius R_0 (at the left boundary). The electron density (n_e), the temperature (T) and the ion concentrations are assumed to be constants in our basic choice of parameters. Only the low field incidence is considered and the results are shown for three minority heating schemes; D(^{3}He), D(H) and T(D). The basic parameters are given in Table I.

Table I **BASIC PARAMETERS FOR THE CALCULATIONS**

	D(^{3}He)	D(H)	T(D)
ω	1.91×10^8 s^{-1}	2.87×10^8 s^{-1}	1.44×10^8 s^{-1}
n_y	0	0	0
n_z	4	4	4
B_0	2.90 T	2.90 T	2.90 T
R_0	3.1 m	3.1 m	3.1 m
$T_e = T_i$	5 keV	5 keV	5 keV
n_e	5×10^{19} m^{-3}	5×10^{19} m^{-3}	5×10^{19} m^{-3}
$n_{^3He}/n_e$	0.03	0	0
n_H/n_e	0	0.03	0
n_D/n_e	0.94	0.97	0.5
n_T/n_e	0	0	0.5
L	0.6 m	0.3 m	0.75 m

With our parameters, the cyclotron resonance lies at $R = 3.0$ m, where the magnetic field is 3 T. The parameters to be altered are n_z, n_y, minority concentration, plasma density, species temperatures, and the reflection coefficient of the transmitted fast wave from the inner wall. Separate effects to be studied include the impurity concentration and the gradient effects.

3.2.1 Minority concentration and n_z

The parameters which most strongly affect the distance between the cyclotron resonance and mode conversion resonance are the species' charge to mass ratios and the species' concentrations. For the minority heating schemes, in this paper, the cut-off and the conversion regime are both on the high field side. The distance between the resonances with our parameters varies between 0 and 54 cm, depending on the scheme, and is roughly proportional to minority concentration ν_m.

Fig. 4 shows the conversion, reflection and transmission coefficients (in power flux) as a

function of n_z for D(H) minority heating scheme. For this particular case we have chosen the parameters of PLT; $\omega = 2.87 \times 10^8$ s^{-1}, $B = 3$ T at $R = 1.3$ m, $T_e = T_H = T_D = 2$ keV, $n_H = 1.5 \times 10^{18}$ m^{-3}, $n_D = 2.85 \times 10^{19}$ m^{-3} and $n_y = 0$. The left boundary is set at $R = 1.4$ m, and $L = 45$ cm. The same case (with a possibly different calculation region) has been calculated by Romero and Scharer [14] and Jaeger et al [5]. We find a good agreement with their calculations, in spite of differences in the codes which have been used.

The prediction given by Eq. (27) is shown in Fig. 4. Note that in the following η is calculated with the real parts of S, D and σ. A good agreement at low n_z and a satisfactory agreement for high n_z is found with the numerical results. We have also calculated the power coefficients from the Budden estimates in Eq. (2) without the slow wave damping correction. While the reflection and transmission seem to be less affected by the damping for the chosen n_z range, the conversion is strongly reduced for large n_z above $n_z \sim 6$. For $n_z = 10$, we find $\mid C \mid^2 = 0.249$ from Eq. (2). The corresponding numerical result from Fig. (4) is 0.04, while Eq. (27) gives 0.175. By integrating Eq. (7) numerically, without linearizing S, with a constant E_y, we find $\mid C \mid^2 = 0.145$. Hence, an almost perfect agreement with the numerical result can be obtained if, in addition, we account for the electron Landau damped fraction of the converted power flux which is about 8% of the total incident power flux. Therefore, we conclude that the Budden formalism in the present case is sufficiently accurate to account for the gross behaviour of the power coefficients provided the slow wave damping for $n_z > 6$ is included according to the theory presented in Sec. 2. The dominant effect of cyclotron damping on conversion is due to the damping of the converted wave, and not that of the fast wave.

Figs. 5, 6 and 7 show the power coefficients for the T(D), D(H) and D(^{3}He) minority heating schemes, with the parameters given in Table I. The results are presented for various minority concentrations and are shown with the predictions given by Eq.(27) for the conversion and by Eq. (2) for the conversion and transmission. We find that the absorption is maximized at large n_z and at intermediate values of minority concentration, as expected from the theory of cyclotron absorption. The transmission reduces for increasing minority concentration, according to the predictions of the tunnelling equation. A satisfactory agreement with the Budden theory can be obtained for small n_z. However, for sufficiently large n_z, η in Eq. (2) can not be estimated accurately from the real parts of S, D and σ, and Eq. (2) fails to give the correct transmission. This can be observed, in particular, for the case of T(D) with $\nu_m = 0.1$ and for the other heating schemes with the minority concentrations shown. Note that the model predicts a zero transmission when the mode conversion resonance disappears (Re(S) becomes less than n_z^2 everywhere).

As expected, the conversion decreases faster with n_z for smaller minority concentrations. For the whole range of parameters we find a satisfactory agreement between the estimate in Eq. (27) and the numerical results for the conversion. For very low concentrations at small n_z we find larger discrepancies, which obviously are due to the rapid variation of S around the resonance and due to the closeness of the mode conversion layer and the cut-off. For D(^{3}He) minority heating scheme with $n_{^3He}/n_e = 0.01$ and $n_z = 2$, $\mid a_1 \mid$ is

of the order of 0.003 which is of the same order as the distance between the resonances ($\sim$ 0.005). This clearly makes the linearization of S or D invalid in our local analysis of Eqs. (7) and (8). For the same reason, the Budden estimates are not accurate in this limit. Note that the Budden estimates can deviate from the numerical results even by 50 % in the whole parameter region. A main part of this deviation follows because the location of the fast wave cut-off is not accurately obtained after linearizing Eq. (12) (see Section 2.1). This leads to an error in $\mid E_y \mid$ at the resonance, and, according to Eq. (24), to an error in the conversion estimate. Due to the particular spatial variation of S and D around the resonance, this makes the Budden estimates usually to underestimate the conversion. For increasing n_z, the damping of the converted wave becomes strong, and the conversion rapidly decreases for low concentrations. This is well predicted by Eq. (27).

Because we underestimate the slow wave damping in linearizing the imaginary part of S near the resonance, the decrease of the conversion for increasing n_z is somewhat delayed in our model. We were able to integrate Eq. (7) with the true S numerically over the resonance, assuming a constant E_y. For the converted power flux obtained in this way, we found a much better agreement with the full numerical solution for large n_z. The clear difference between the analytical and numerical curves for large n_z in the shown regime, obtained for the case of DT-plasma with high minority concentration ($\nu_D \geq 20\%$), can be explained by the electron Landau damping of the slow wave, which is not taken into account in our analytical theory. In fact, by artifically setting P real in our numerical computations, a good agreement with the analytical curves was found for $\nu_D \geq 20\%$ in the depicted parameter region. We also note that Eq.(24) works better than Eq. (27), if the solution for E_y from the numerical calculations is substituted into Eq. (24). This demonstrates the error in the solution for E_y which arises due to the linearization of Eqs. (7) and (8).

3.2.2 Plasma density and temperature

For the ion-ion hybrid resonances, the distance between the fast wave cut-off and resonance is roughly independent of the plasma density or temperature, while η in the Budden solution increases with density. For a low density, we expect the conversion to increase with density while for higher densities to decrease with density. As a function of the temperature, the conversion at ion-ion hybrid resonances should remain relatively constant in the region where the cyclotron resonance is well separated from the conversion region, i.e $\mid n_z \mid v_{Ti}/c < (1/2)\nu_m$. These expectations are verified by the numerical calculations, the results of which are shown in Figs. 8 and 9. Here we have altered the density and temperature for the schemes defined in Table I. The results are shown together with the conversion estimate given by Eq. (27). The effect of density on the coefficients is well described by the Budden theory, and the dependence on temperature is satisfactorily well described by the theory in Section 2. The large difference between the numerical and analytical conversion fraction at low densities in Fig. 8a is due to the electron Landau damping of the slow wave. In the case of Fig. 8a, n_z is large, and the increase of E_z with decreasing density causes the Landau damping to be enhanced for the converted wave.

By adding the Landau damped fraction of the incident power flux to the numerically obtained conversion fraction, an excellent agreement with Eq. (27) can be obtained for the low densities, too, in the present case.

Fig. 10 shows the dependence on the minority temperature with fixed majority temperature. No essential changes, with respect to the case with equivalent temperature for each species, can be found. In Figs. 8-10 we have kept the electron temperature fixed ($T_e = 5$ keV). For these cases $n_z v_{Te}/c$ is usually less than one, and weak electron Landau damping and Transit Time damping results. In Fig. 11 we show the dependence of the power coefficients on the electron temperature with fixed ion temperature. The results indicate no large variations, which supports our model where the major temperature effect on the conversion is due to the ion cyclotron damping of the converted wave. It is also concluded that the ion Bernstein wave has a weak electron Landau damping in the shown temperature region. Note, however, the nonnegligible electron Landau damping obtained for the parameters in Figs. 4, 5 and 8a. We also remind that corrections to next order in electron Larmor radius may be needed to correctly describe the damping of the ion Bernstein wave at very high temperatures ($T_e > 10$ keV) [26].

3.2.3 Poloidal refractive index n_y

We note that the coefficient of E_y in Eq. (28) can be given by $i\delta(n_x^2 + n_y^2) + n_x n_y - iD$ in the WKB limit. For the parameters relevant at the plasma centre this is dominated by $-iD$, if n_x is replaced by the fast wave wavenumber. Because E_y is very small for the slow waves according to Eq. (29) we do not expect large effects of n_y on the conversion. Our numerical results for the power coefficients in the range $\mid n_y \mid = 0 - 2$ indicated no larger variation than 1%. We remind that the conversion at the resonances situated near the plasma edge are strongly affected by n_y due to the $n_y n_x$ term in the coefficient of E_y in Eq. (28) [27].

3.2.4 Impurities

Various light impurities like Be, O or C may exist at the plasma centre to a large abundance. Because Ω_{Be} and Ω_O are somewhat smaller than Ω_D, we expect the ion-ion hybrid resonance for the T(D) minority heating scheme to be affected by the impurities. Fig. 12 shows the graphs of S around the resonance for this case with and without beryllium. The nearly isolated D-T ion-ion hybrid resonance is replaced by a couple of resonances formed by the impurity and the two major constituents. In Fig. 13 we show the power coefficients as a function of n_z and minority concentration for the T(D) heating scheme with 5% beryllium concentration and with the same parameters as in Fig. 5. Fig. 14 shows the coefficients as a function of beryllium concentration with $n_z = 10$. We do not give here any analytical predictions, although it would be possible to connect the scattering and transmission coefficients at the two resonances to find out the combined effect. With respect to the results shown in Fig. 5, large effects of the impurity can be

found for the absorption and the transmission coefficients at high concentrations and for large n_z. Significant changes in the conversion coefficient can be found for all the shown concentrations at large n_z.

3.2.5 Wall reflection

A nonnegligible transmission of power through the resonance-pair may produce cavity modes with a complex field pattern over the cross-section of the plasma torus. Because of the rapidly changing $\mid E_y \mid$, with consecutive minima and maxima in radial and poloidal directions, the conversion coefficient varies strongly as a function of the spatial location. In this case Eq. (27) is not valid, if a sufficiently collimated and intense reflection from the walls takes place. Instead, Eq.(24) should be used to find the local absorption. For multiple reflections in non-circular tokamaks, the phase of E_y may well be described by a random-phase approximation, and the connection of the average value of $\mid E_y \mid^2$ to the net power coupled by the antenna should be known. This is probably best done with two-dimensional codes like LION [6] and will not be discussed further.

The effect of the wall reflection on the conversion coefficient is demonstrated by assuming a reflected fast wave at the right boundary in our code. Fig. 15 shows the conversion coefficient as a function of the relative phase change between the outgoing and incoming fast wave branches at the right boundary. We have chosen D(^{3}He) minority heating scheme and assume equal amplitudes for the outgoing and incoming modes. A good agreement with the prediction given by Eq. (24) is found, which supports the idea of separating the effect of $\mid E_y \mid$ in the conversion formula. The deep minima in conversion point out the importance of the effect of cavity modes on the conversion. However, we note that for the case of relatively strong single-pass absorption the reflected wave from the inner wall is weak and may lose its amplitude further by beam divergence effects in non-circular tokamaks. In that case, the conversion coefficient (averaged over the resonance surface) should be well described by Eq. (27).

3.2.6 Gradients of background plasma

To test the validity of the predictions in Eqs. (24) and (27), it is important to alter the gradients of the plasma parameters, too. From the formulae we expect the gradients of D and S to be of major importance. However, when we compare our model equations (7) and (8) to the full wave equations (28)-(30) in our code we would expect the gradients of the kinetic corrections to play some role. In Figs. 16 and 17 we show the power coefficients as a function of ∇n_e and ∇T with the parameters given in Table I. We find some deviations from the prediction in Eq. (27) for large ∇T. This is because the gradients of σ become large in this limit and the integration of Eq. (7), as it was done in Sec. 2, becomes less accurate. As a function of the density gradient ∇n_e, the deviations are larger. For the T(D) case we find a reduction in conversion for the large gradient, which is due to the decrease in the distance between the cyclotron resonance and the

conversion layer which makes the Doppler-effect stronger. For the other schemes, we do not find any pronounced effect of the density gradient on the conversion with the chosen parameters. Note that the temperature and density are fixed at the left boundary in Figs. 16 and 17. Hence, if the gradients increase, their values decrease at the resonance. For the T(D) and D(^{3}He) cases, the resonance lies relatively close to the left boundary so that the decrease in n_e and T at the resonance is largest for the D(H) case.

4 Conclusions

We have derived an analytical estimate for the mode converted power fraction of the incident fast wave in the presence of ion cyclotron damping. The estimate is valid for any strength of damping and is obtained by integrating the slow wave equation over the resonance region assuming a constant fast wave drive. The conversion fraction is found to be a function of the amplitude of the local fast wave electric field, local plasma parameters and their gradients. The different scale lengths of the fast wave and slow wave variation make it possible to separately consider the effects of the fast wave drive and slow wave damping on the conversion, as well as the mechanisms affecting the fast wave.

The conversion is reduced for increasing ion cyclotron damping of the slow wave and for decreasing fast wave field amplitude at the resonance. We show in Fig. 18 the absorption profile for the T(D) case at $n_z = 6$, where the cyclotron damping is not sufficiently strong to attenuate the slow wave, and at $n_z = 10$, where a significant damping of the slow wave exists. We find that the decrease in the conversion from $n_z = 6$ to $n_z = 10$ (see Fig. 5c) actually appears as a local increase in cyclotron damping at the resonance. From the present analysis we are not able to predict what happens to the resonance absorption as a whole when n_z or T increases. The conversion fraction given by Eq. (27) is the fraction of the resonance absorption which converts to the energy flux of the propagating slow wave and will be damped by other mechanisms than ion cyclotron damping near the resonance. Therefore, to first approximation that estimate can be used to evaluate the electron damping arising from the conversion.

The fast wave field is relatively insensitive to the conversion process but may be strongly affected by the length of the evanescent region in front of the resonance as well as by the cavity effects. The present analysis shows that the conversion takes place in a very narrow region around the resonance, the extent of which is determined to be of the order of $(\sigma/S')^{1/3}$. This is usually much less than the fast wave wavelength. The validity of our results presupposes that the linearization of the parameters around the resonance is valid over this length. This is also a necessary condition for the validity of the Budden or tunnelling solutions.

The analysis in Ref. [20] is based on the use of second-order equations by treating the slow wave as a driven response to the fast wave. We note that this approximation, which is used to simplify the numerical calculations of the conversion, derives its origin from the separability of the fast and slow wave behaviour, as demonstrated in the present

paper. We note that the model used in our paper is applicable to the ion-ion hybrid resonances, the Alfvén resonance [24] and to the lower hybrid resonance [27] in the ion cyclotron range of frequencies. In the case of harmonic resonances, where the second-order equations (7) and (8) are not complete, this model is not valid. However, it should be noted that the theory of Kay *et. al* [20] has been applied with success in this case, too. We believe that a similar analytical theory, as ours, can be derived for the case of harmonic resonances from a more complete system of equations.

We have compared our analytical results to the numerical solution of the full wave equations, valid to second order in ion Larmor radius, for various minority heating schemes, assuming inhomogeneous plasma parameters. A satisfactory agreement is found for a large range of parameters n_z, n_y, ν_m, plasma density and temperature. The largest discrepancies are found when the cyclotron resonance and the hybrid resonance are close to each other, which invalidates any linearization of the parameters in the conversion regime. However, we note that deviations as large as 50 % are common for the whole parameter range. For large n_z or large T, this follows from the incapability of our damping model to fully simulate the cyclotron damping of the slow wave. For the case of weak damping, the linearization of the plasma parameters, used for the Budden and tunnelling model, fails to give accurately the location of the fast wave cut-off. The consequent error in $\mid E_y \mid$ at the resonance leads usually to an underestimate of the conversion coefficient. The magnitude of the error depends sensitively on the precise value of η and the plasma parameters. However, one should note that the direct dependence of the conversion on $\mid E_y \mid$ at the resonance, as predicted by Eq. (24), makes the conversion coefficient to depend on many effects not described by the one-dimensional theory. An important effect of cavity formation on the conversion by its influence on the local fast wave electric field demonstrates the care which one has to use in exploiting the analytical estimates.

ACKNOWLEDGEMENTS

This work was done under the JET Contract No. JT9/13569 at the Technical Research Centre of Finland and Helsinki University of Technology. The authors wish to thank Dr.D.F. Düchs for his support and encouragement during this work. We also thank Dr. L.-G. Eriksson for suggestions and interest in the course of this work.

The authors are also grateful to Prof. R.R.E Salomaa and Dr. S.J. Karttunen for their interest and support to this work.

References

[1] Fukuyama, A., Nishiyama, S., Itoh, K. and Itoh, S.-I., Nuclear Fusion **23**, 1005 (1983).

[2] Colestock, P.L. and Kashuba, R.J., Nuclear Fusion **23**, 763 (1983).

[3] Chiu, S.C. and Mau, T.K., Nuclear Fusion **23**, 1613 (1983).

[4] Appert, K., Hellsten; T., Vaclavik, J., and Villard, L., Comp. Phys. Comm. **40**, 73 (1986).

[5] Jaeger, E.F., Batchelor, D.B. and Weitzner, H., Nuclear Fusion **28**, 53 (1988).

[6] Villard, L., Appert, K., Gruber, R. and Vaclavik, J., Comp. Phys. **4**, 95 (1986).

[7] Brambilla, M. and Krücken, T., Nuclear Fusion **28**, 1813 (1988); Brambilla, M., Plasma Phys, Contr. Fusion **31**, 723 (1989).

[8] Jaeger, E.F., Batchelor, D.B., Carter, M.D. and Weitzner, H., Nuclear Fusion **30**, 505 (1990).

[9] Stix, T.H. and Swanson, D.G., in "Handbook of Plasma Physics", Ed. by A.A. Galeev and R.N. Sudan, North-Holland Publishing Company (1983) Vol.I, Ch.2.4.

[10] Stix, T.H., Phys. Rev. Lett. **15**, 878 (1965)

[11] Budden, K.G., "Physics of the Ionosphere", Physical Society, London (1955) p.320.

[12] Erokhin, N.S. and Moiseev, S.S., Reviews of Plasma Physics (Consultants Bureau, New York, 1979), Vol.7, p.181.

[13] Ngan, Y.C. and Swanson, D.G., Phys. Fluids **20**, 1920 (1977).

[14] Romero, H. and Scharer, J., Nuclear Fusion **27**, 363 (1987).

[15] Fuchs, V., Ko, K. and Bers, A., Phys. Fluids **24**, 1251 (1981); Cairns, R.A. and Lashmore-Davies, C.N., Phys. Fluids **26**, 1268 (1983); Fuchs, V., Bers, A. and Harten, L., Phys. Fluids **28**, 177 (1985).

[16] Weynants, R.R., in: Heating in Toroidal Plasmas (Proc. 4th. Int. Symp., Rome 1984), Vol.1, 211.

[17] Swanson, D.G., Phys. Fluids **28**, 2645 (1985).

[18] Chow,C., Fuchs, V. and Bers, A., Phys. Fluids **B2**, 2185 (1990).

[19] Swanson, D.G., Nuclear Fusion **20**, 949 (1980).

[20] Kay, A., Cairns, R.A. and Lashmore-Davies, C.N., Plasma Phys. Contr. Fusion **30**, 471 (1988); Cairns, R.A. and Fuchs, V., Phys. Fluids **B 1(2)**, 350, (1989).

[21] Swanson, D.G. and Ngan, Y.C., Phys. Rev. Lett. **35**, 517 (1975); Swanson, D.G., Phys. Rev. Lett. **36**, 316 (1976); Jacquinot, J., McVey,B.D. and Scharer, J.E., Phys. Rev. Lett. **39**, 88 (1977).

[22] Heikkinen, J.A. and Alava, M.J., Plasma Phys. Contr. Fusion **33**, 397 (1991).

[23] White, R.B. and Chen, F.F., Plasma Phys. **16**, 565 (1974).

[24] Heikkinen, J.A., Hellsten, T. and Alava, M.J., Nuclear Fusion **31**, 417 (1991); Alava, M.J. and Heikkinen, J.A., JET-IR(90)14, JET Joint Undertaking, Abingdon (1990), unpublished.

[25] Brambilla, M. and Ottaviani, M., Plasma Phys. Contr. Fusion **27**, 1 (1985).

[26] Brambilla, M., Nuclear Fusion **28**, 549 (1988).

[27] Alava, M.J. and Heikkinen, J.A., submitted for publication.

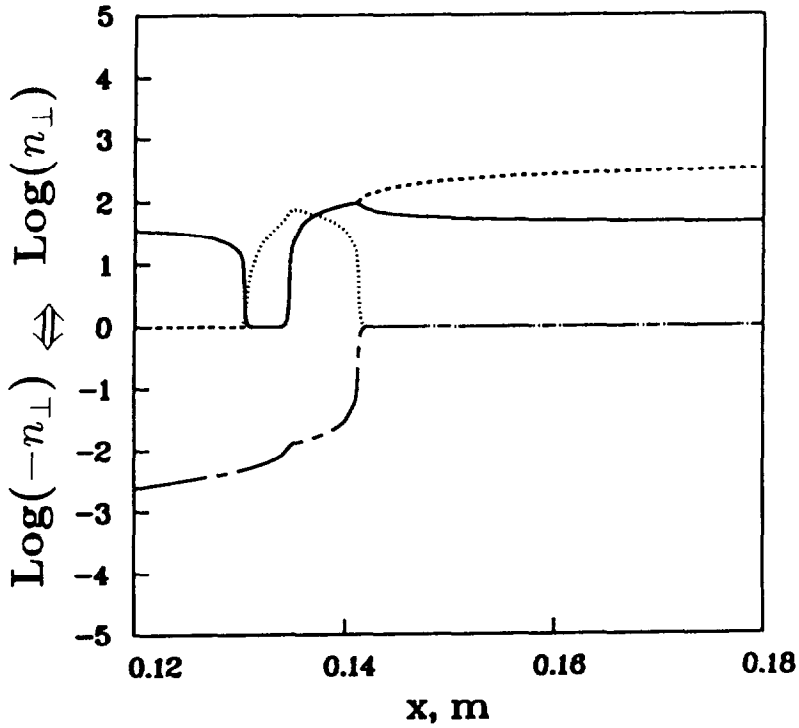

Fig.1 The refractive indices of the fast wave (real part: solid line, imaginary part: dotted line) and ion Bernstein wave (real part: dashed, imaginary part: chain dashed) modes near the ion-ion hybrid resonance as a function of position along the midplane. $x = 0$ is located at 3.1 m, and the high field side is to the right. 5 % ^{3}He in D; $n_z = 2$. The density and temperature are constant with the values 5×10^{19} m^{-3} and 5 keV, respectively.

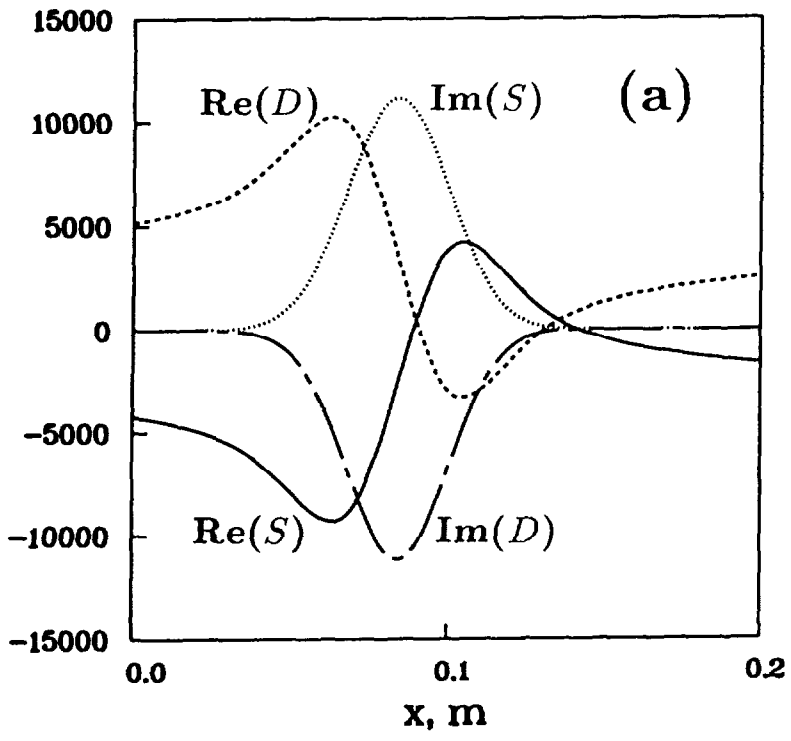

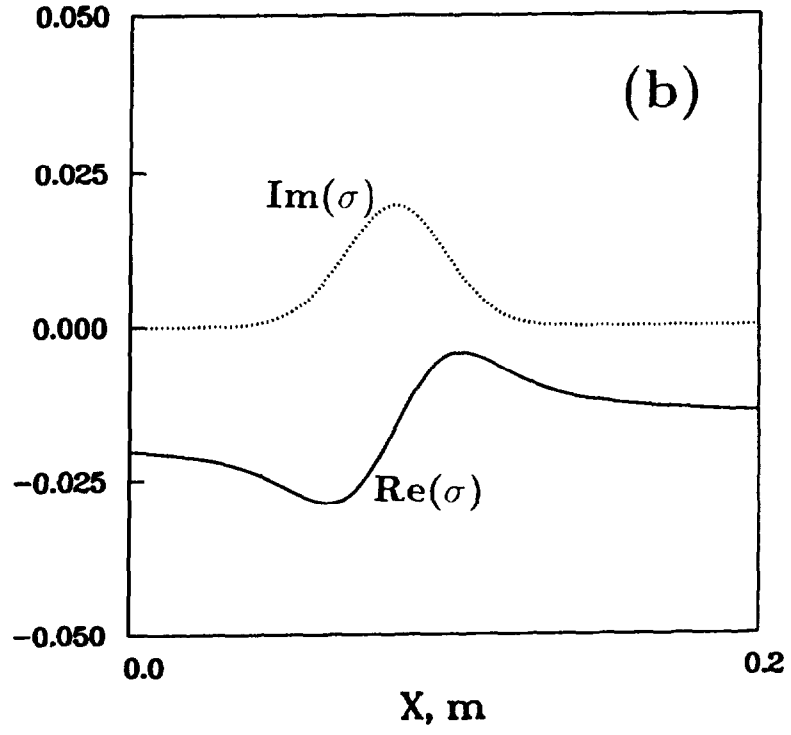

Fig.2 a) S, D and b) σ as a function of position for the same case as Fig. 1 with $n_z = 4$.

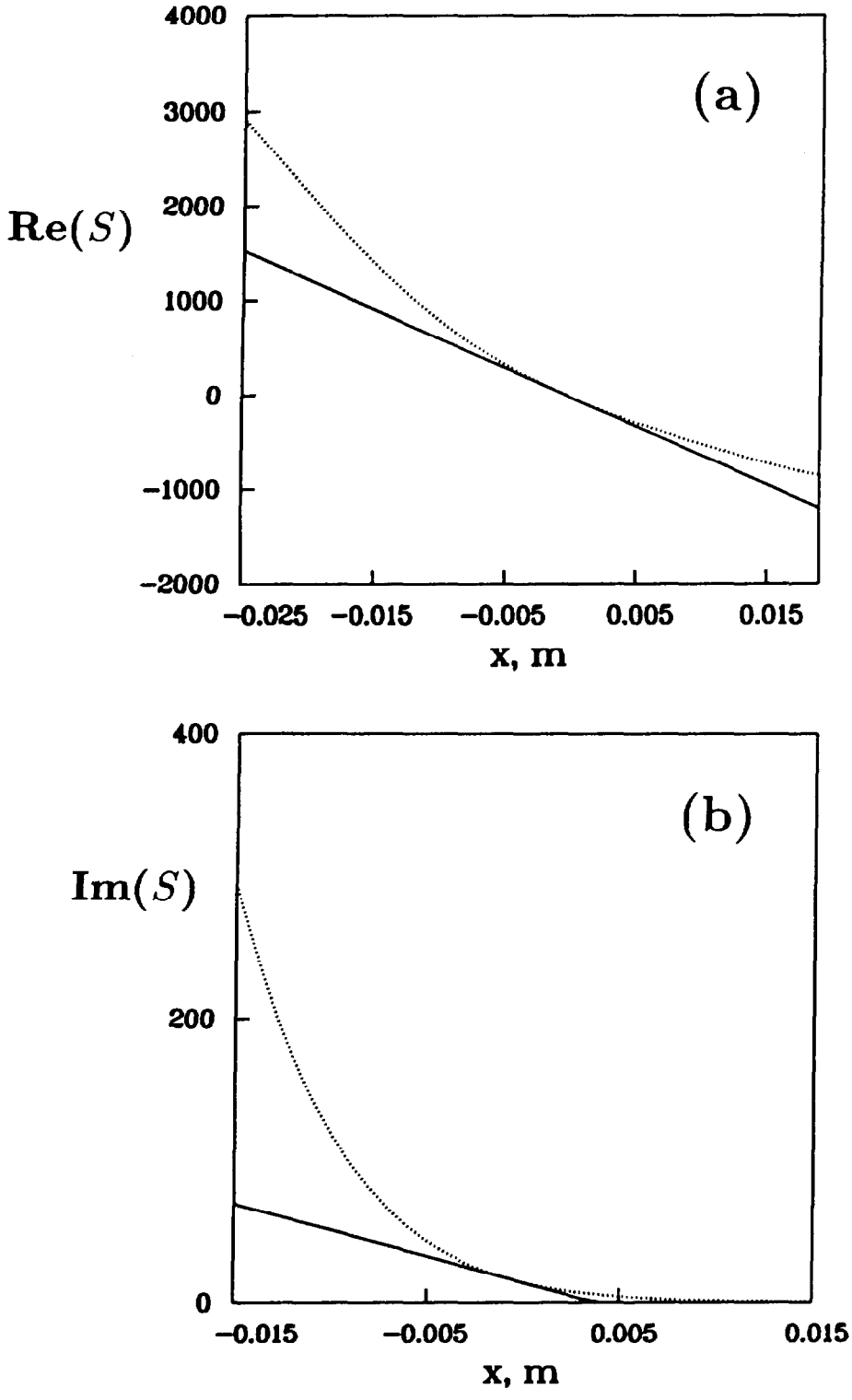

Fig.3 An example of the linearization of S. The mode conversion resonance is at $x = 0$. The dotted line gives the correct behaviour and the solid line the model curve. a) real part; b) imaginary part. The imaginary part is linearized in two parts so that the slope of the non-constant part equals the derivative of the imaginary part of S at the resonance.

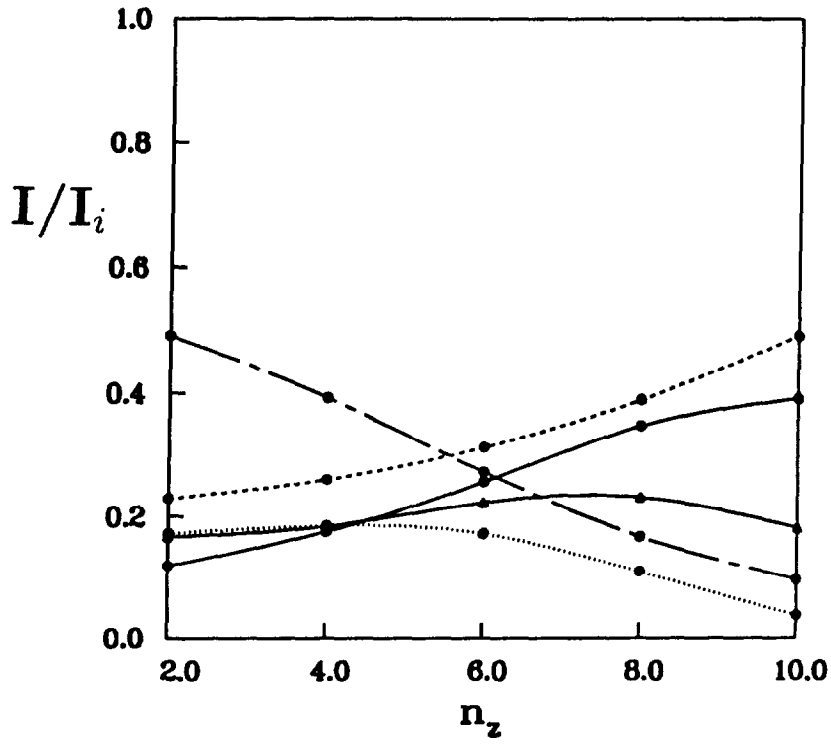

Fig.4 A test case for PLT parameters (see the text). Solid curve with dots: total absorption as a function of n_z. Dotted curve: mode converted part of the total incoming power. Dashed curve: transmitted power. Chain dashed one: reflected power. Solid with triangles: analytical estimate from Eq.(27).

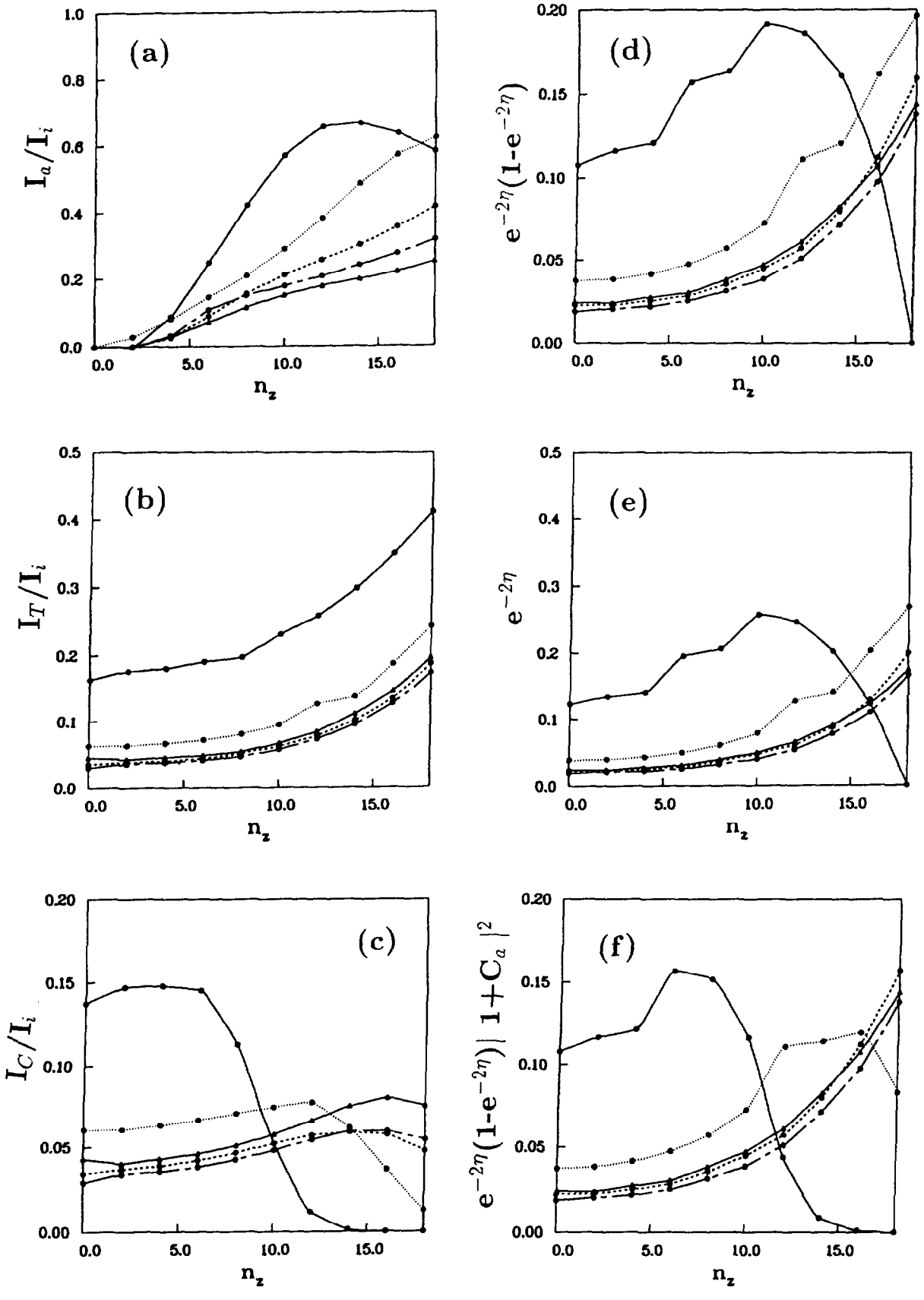

Fig.5 The power coefficients as a function of n_z for a T(D) heating scheme. Solid curve: $\nu_D = 0.1$, dotted: $\nu_D = 0.2$, dashed: $\nu_D = 0.3$, chain dashed: $\nu_D = 0.4$ and solid with triangles as markers: $\nu_D = 0.5$. a) absorbed power; b) transmitted power; c) converted power; d) the Budden estimate for the converted power; e) the Budden estimate for the transmitted power; f) the Budden estimate for the converted power including the damping (Eq.(27)).

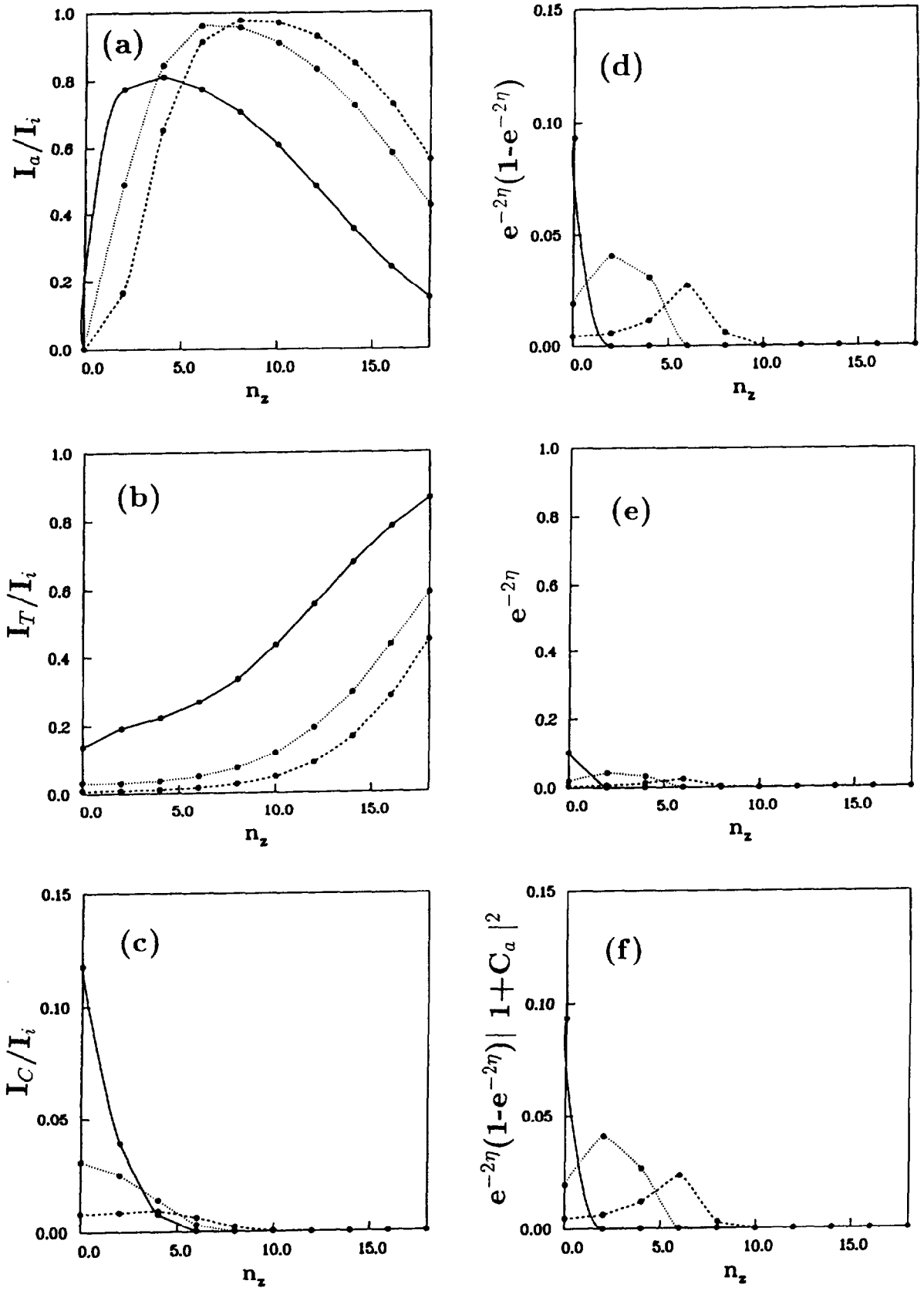

Fig.6 The power coefficients as a function of n_z for a D(H) heating scheme. Solid curve: $\nu_H = 0.01$, dotted: $\nu_H = 0.03$, dashed: $\nu_H = 0.05$. a) absorbed power; b) transmitted power; c) converted power; d) the Budden estimate for the converted power; e) the Budden estimate for the transmitted power; f) the Budden estimate for the converted power including the damping (Eq.(27)).

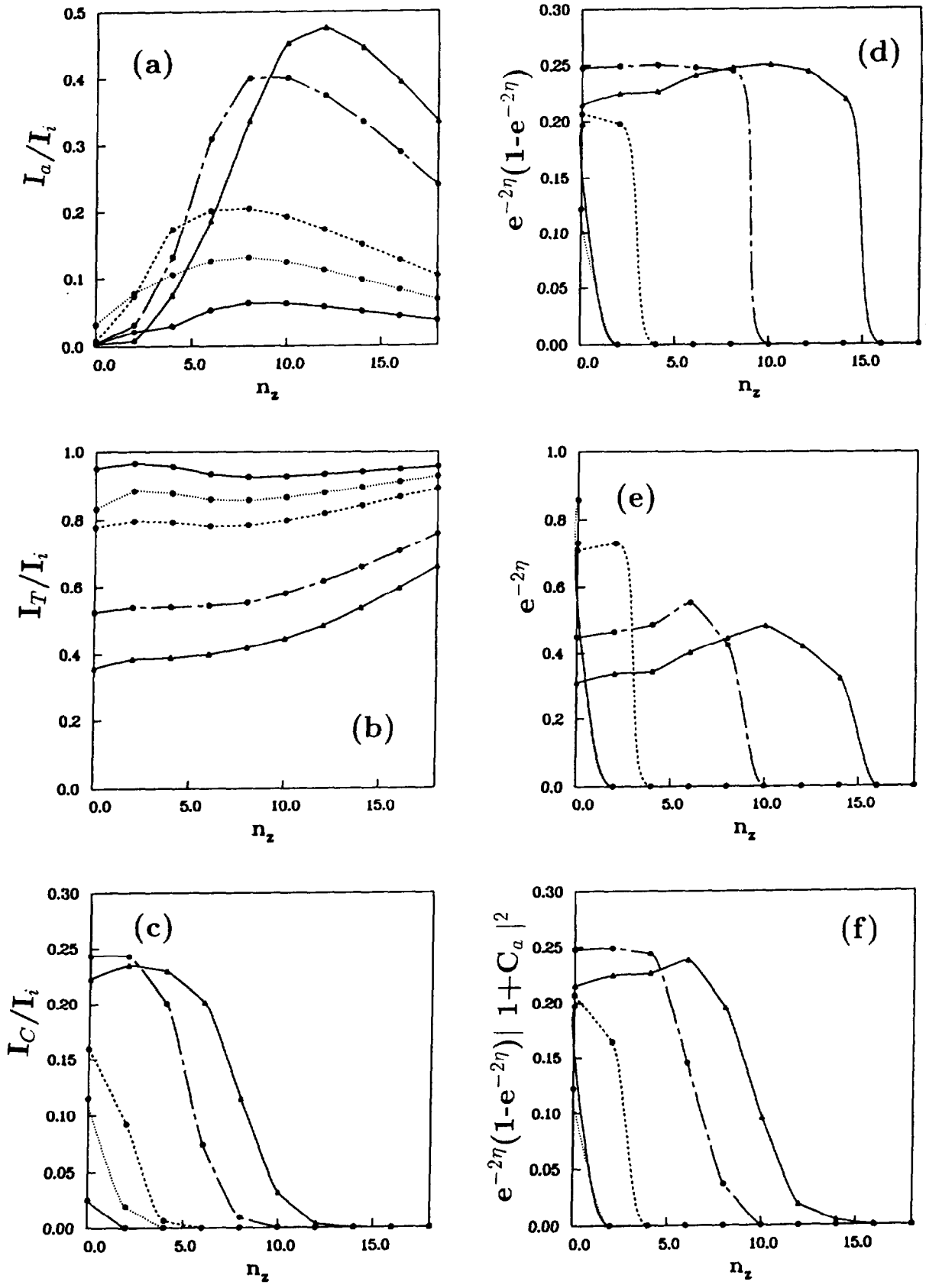

Fig.7 The power coefficients as a function of n_z for a D(^{3}He) heating scheme. Solid curve: $\nu_{^3He} = 0.001$, dotted: $\nu_{^3He} = 0.005$, dashed: $\nu_{^3He} = 0.01$, chain dashed: $\nu_{^3He} = 0.03$ and solid with triangles as markers: $\nu_{^3He} = 0.05$. a) absorbed power; b) transmitted power; c) converted power; d) the Budden estimate for the converted power; e) the Budden estimate for the transmitted power; f) the Budden estimate for the converted power including the damping (Eq.(27)).

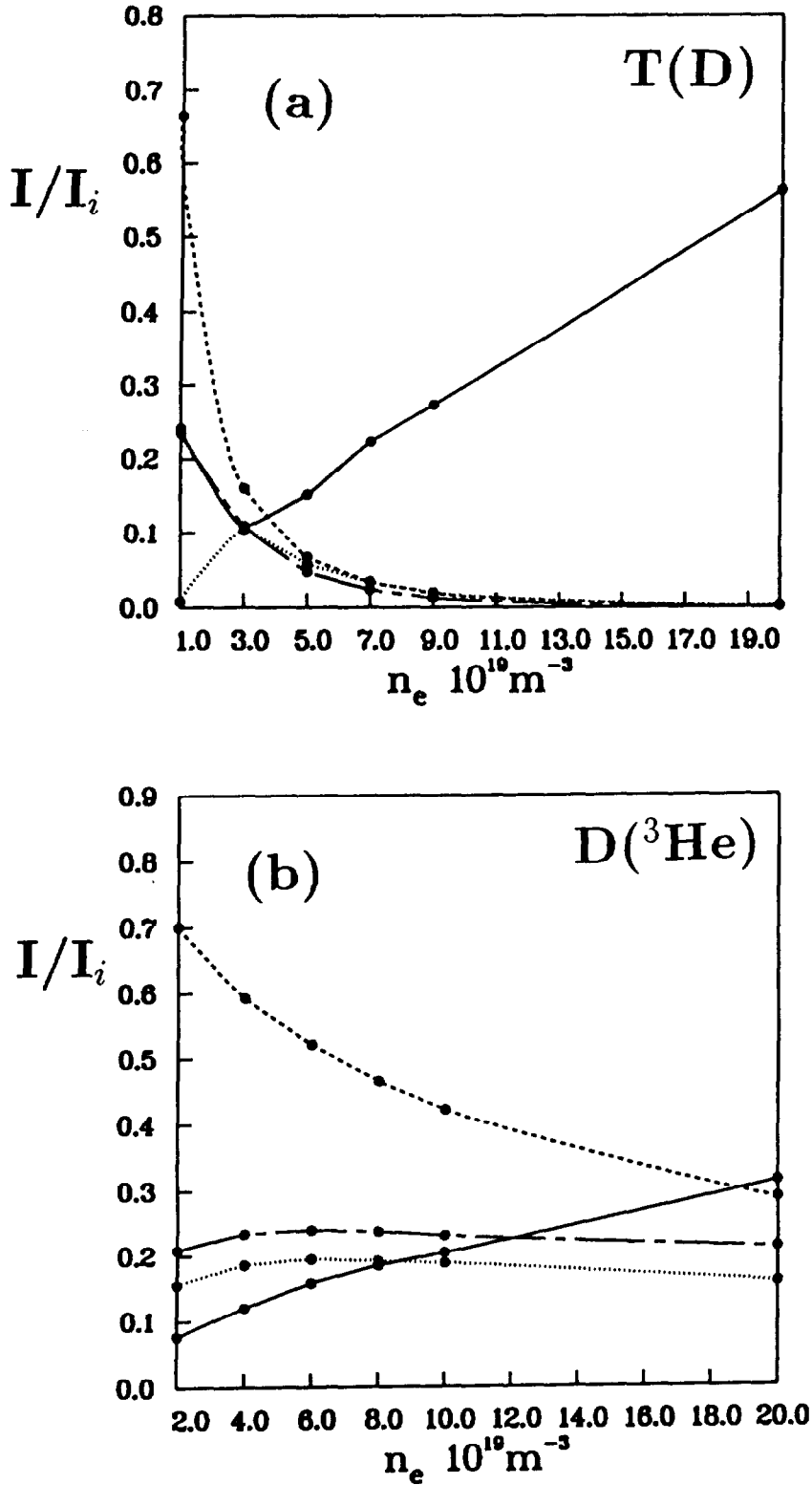

Fig. 8 The effect of varying the density on absorption (solid curve), conversion (dotted) and transmission (dashed). Included is the conversion estimate from Eq.(27) (chain dashed). a) the T(D) heating scheme with $n_z = 10$ and $\nu_D = 0.5$; b) the D(^{3}He) heating scheme with $n_z = 4$ and $\nu_{^3He} = 0.028$; c) the D(H) heating scheme with $n_z = 4$ and $\nu_H = 0.03$.

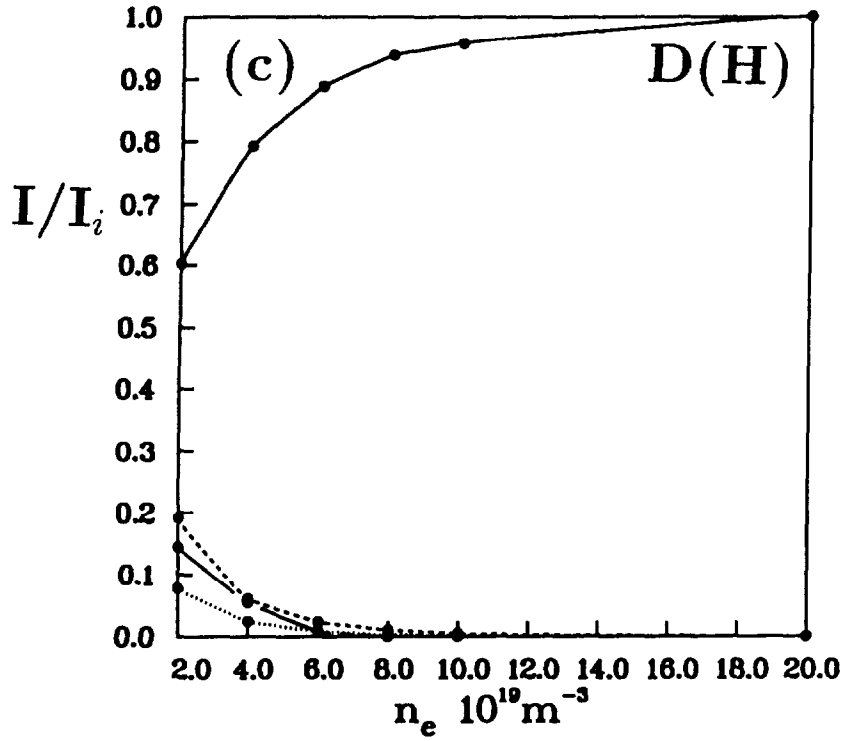
(c)
D(H)
I/I_i
1.0
0.9
0.8
0.7
0.6
0.5
0.4
0.3
0.2
0.1
0.0
2.0 4.0 6.0 8.0 10.0 12.0 14.0 16.0 18.0 20.0
n_e 10^19 m^-3

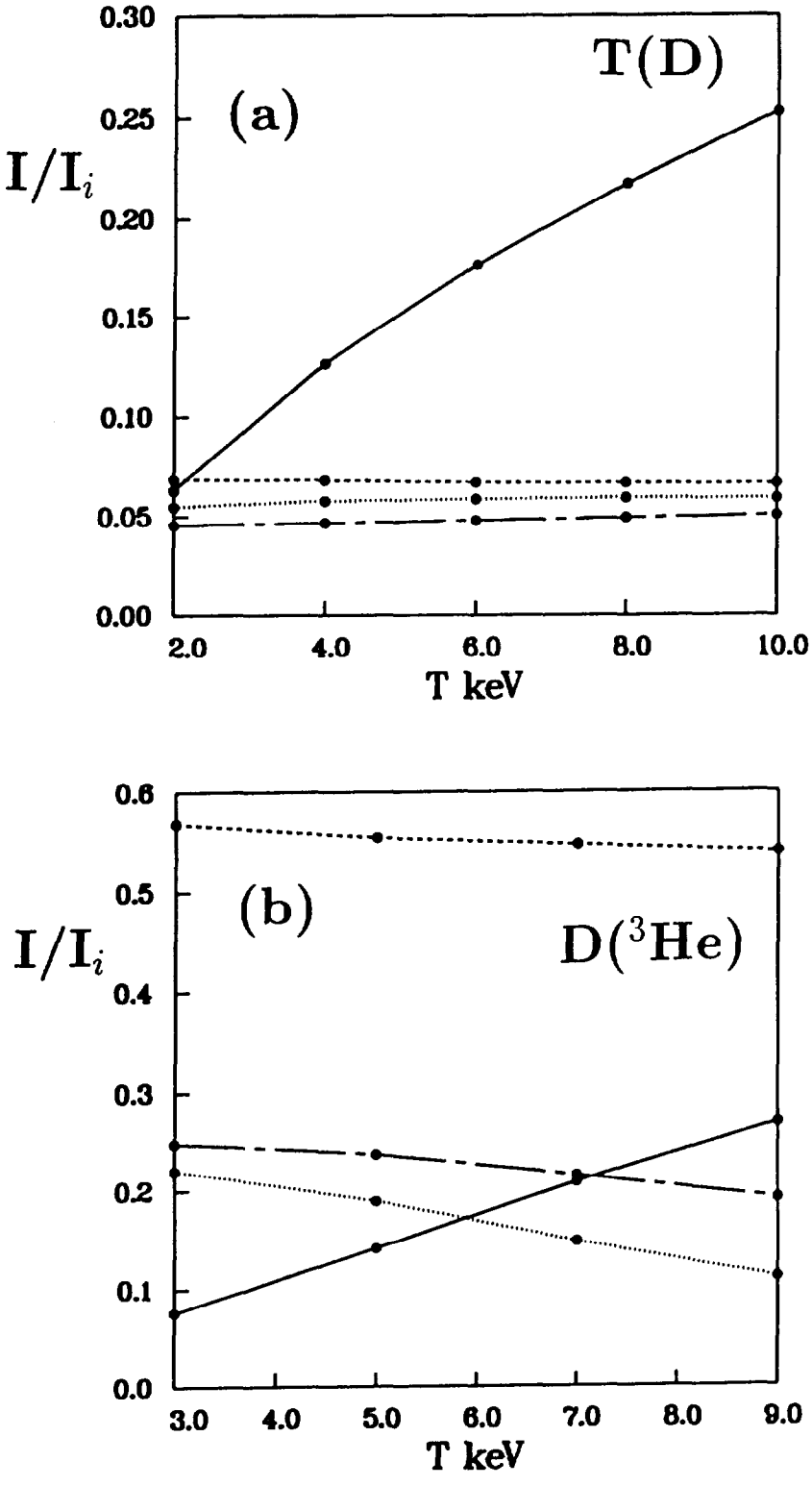

Fig. 9 The effect of varying the temperature on absorption (solid curve), conversion (dotted) and transmission (dashed). Included is the conversion estimate from Eq.(27) (chain dashed). a) the T(D) heating scheme with the same parameters as in Fig.8a; b) the D(^{3}He) heating scheme with the parameters of Fig.8b; c) the D(H) heating scheme with the parameters of Fig.8c.

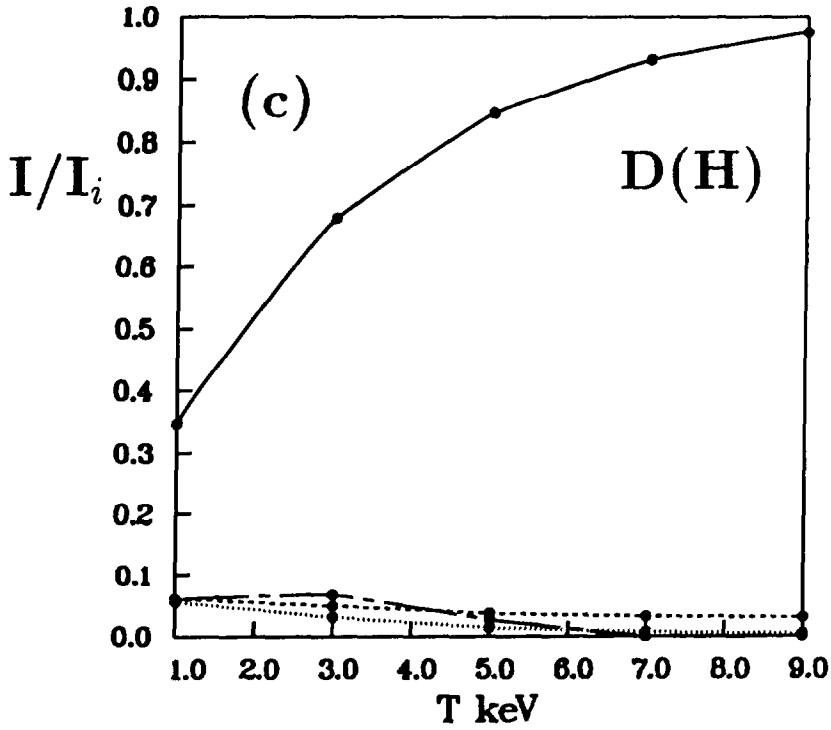
(c)
D(H)
I/I$_i$
1.0
0.9
0.8
0.7
0.6
0.5
0.4
0.3
0.2
0.1
0.0
1.0
2.0
3.0
4.0
5.0
6.0
7.0
8.0
9.0
T keV

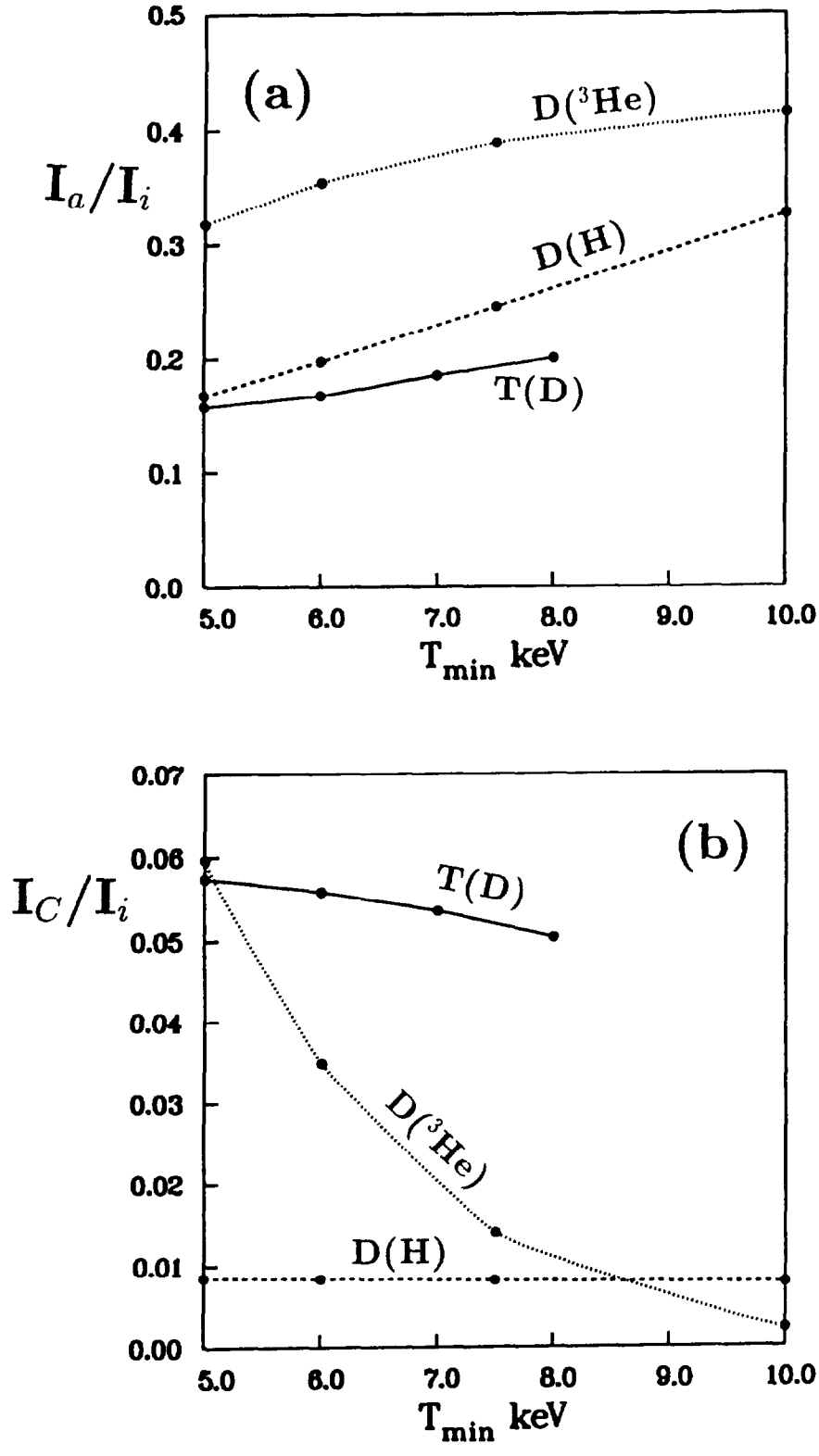

Fig. 10 The effect of minority temperature at a constant majority ion temperature on a) the absorbed power; b) the converted power; c) the transmitted power. The T(D) case ($n_z = 10$, $\nu_D = 0.5$) is presented with a solid line, the D(^{3}He) ($n_z = 6$, $\nu_{^3He} = 0.028$) one with a dotted line, and the D(H) ($n_z = 2$, $\nu_H = 0.05$) one with a dashed line.

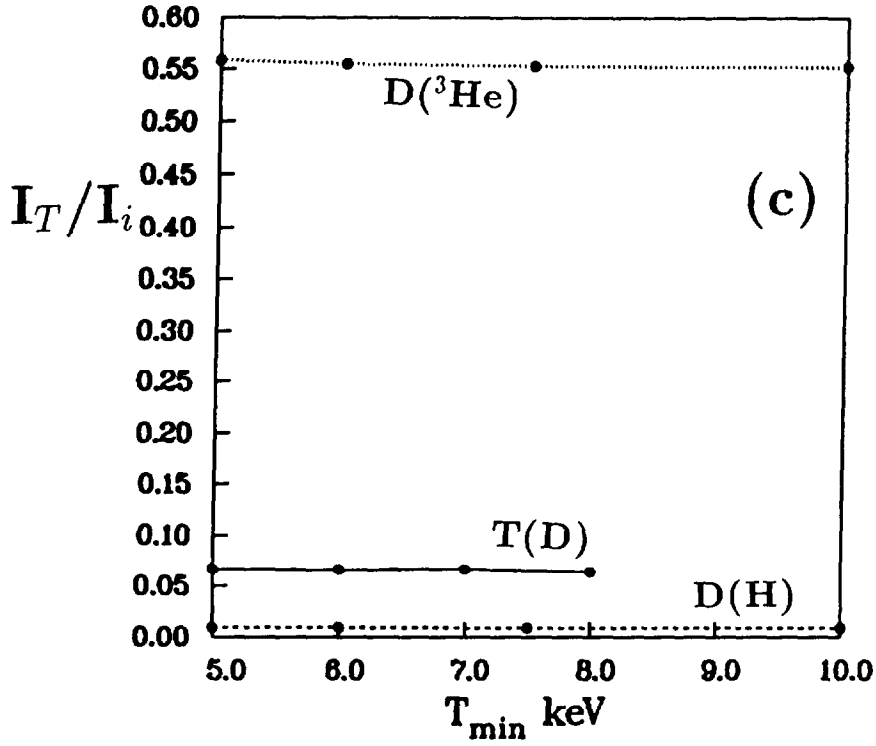
0.60
0.55
0.50
0.45
0.40
0.35
0.30
0.25
0.20
0.15
0.10
0.05
0.00
I_T/I_i
D(^{3}He)
(c)
T(D)
D(H)
5.0
6.0
7.0
8.0
9.0
10.0
T_{min} keV

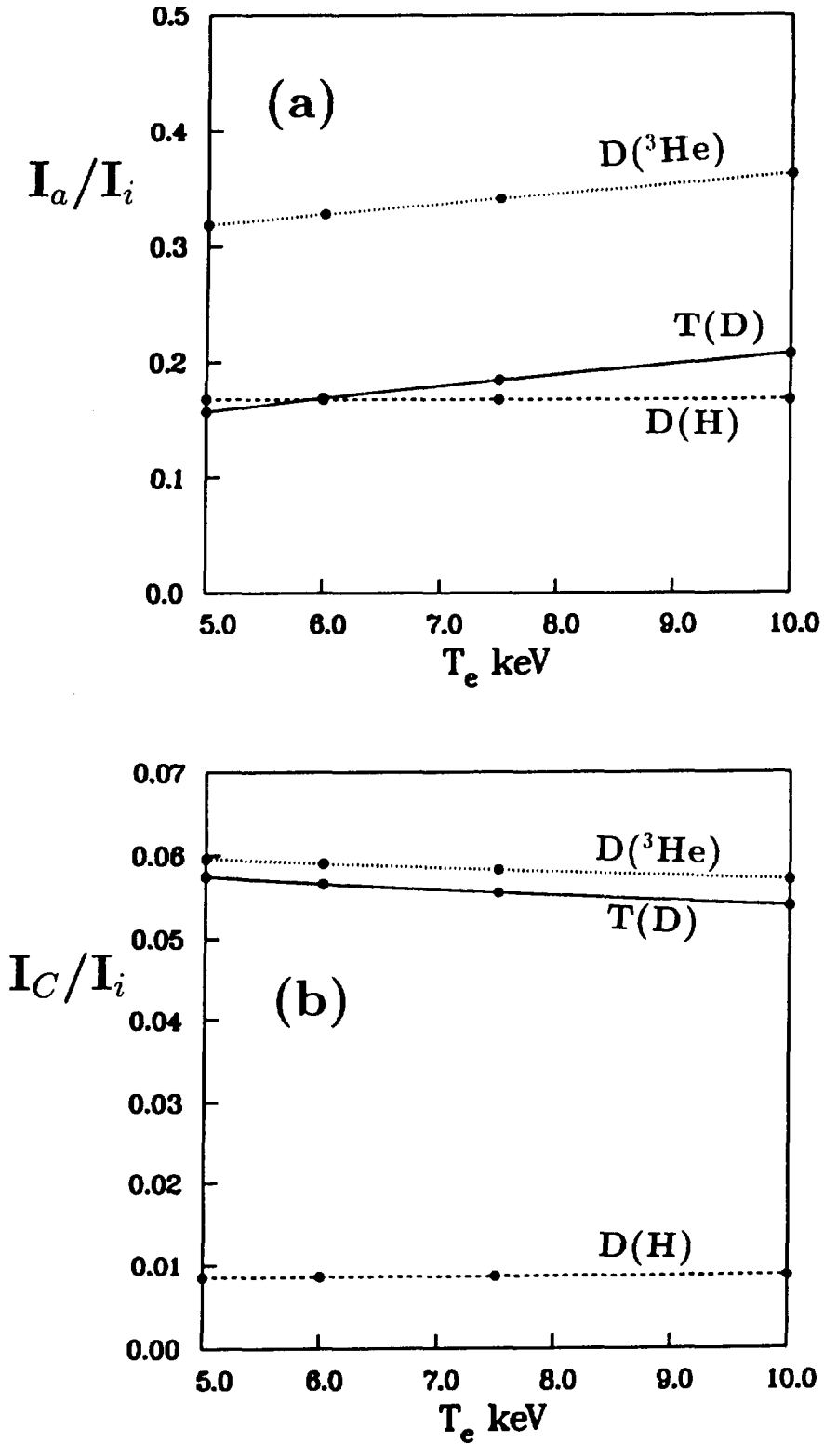

Fig. 11 The effect of the electron temperature at a constant ion temperature on a) the absorbed power; b) the converted power; c) the transmitted power. The T(D) case (n_z = 10) is presented with a solid line, the D(^{3}He) (n_z = 6) one with a dotted line, and the D(H) (n_z = 2) one with a dashed line. Minority concentrations as in Fig.10.

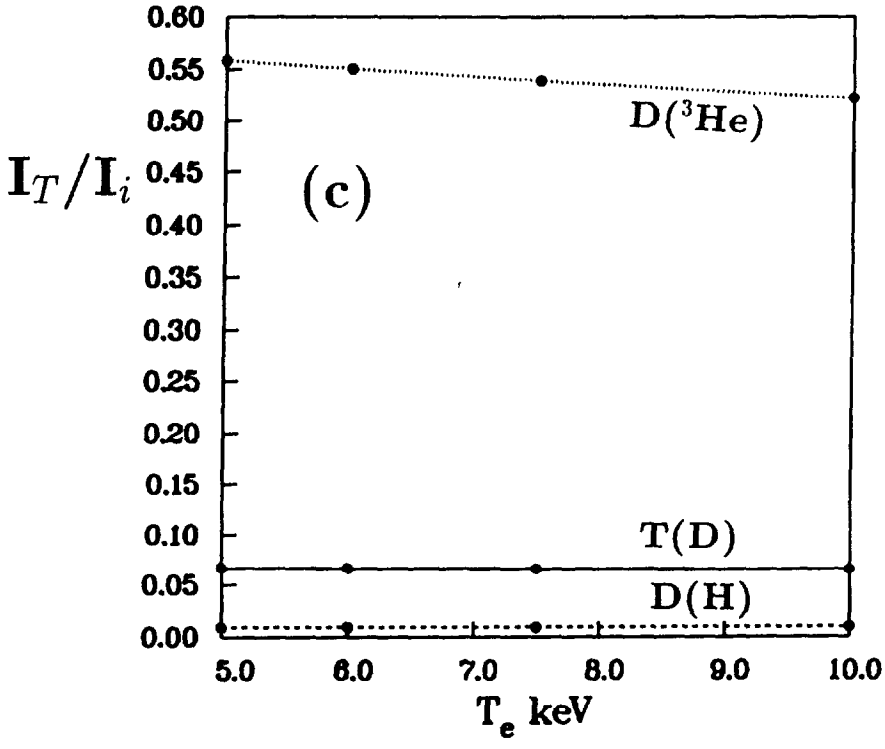
0.60
0.55
0.50
0.45
0.40
0.35
0.30
0.25
0.20
0.15
0.10
0.05
0.00
I_T/I_i
(c)
D(^{3}He)
T(D)
D(H)
5.0
6.0
7.0
8.0
9.0
10.0
T_e keV

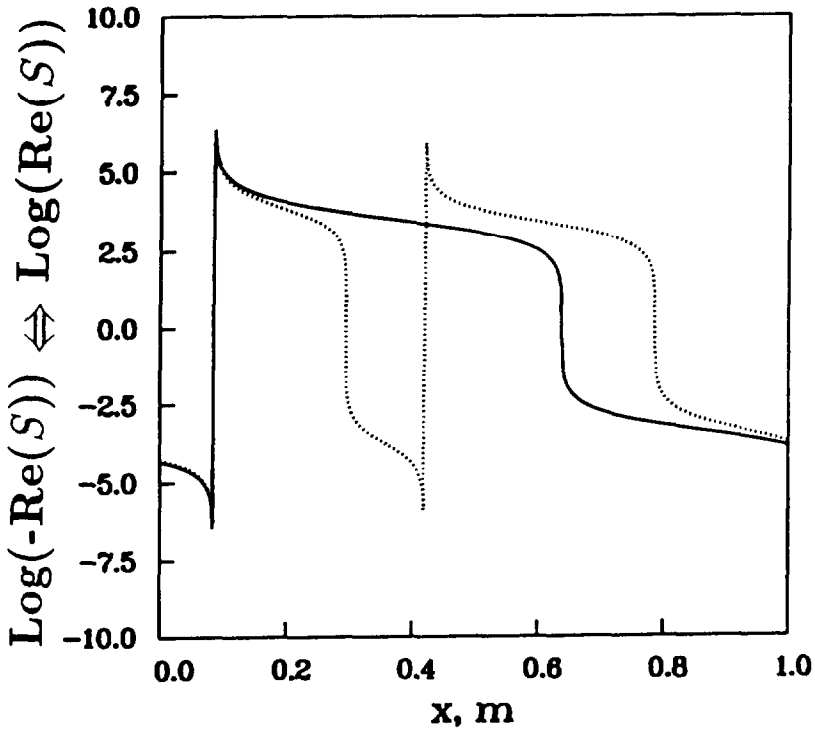

Fig. 12 The solid curve shows the logarithm of S as a function of position from $R = 3.1$ m to the high field side for a pure 50–50 % T(D) plasma, and the dotted one with 5 % of beryllium.

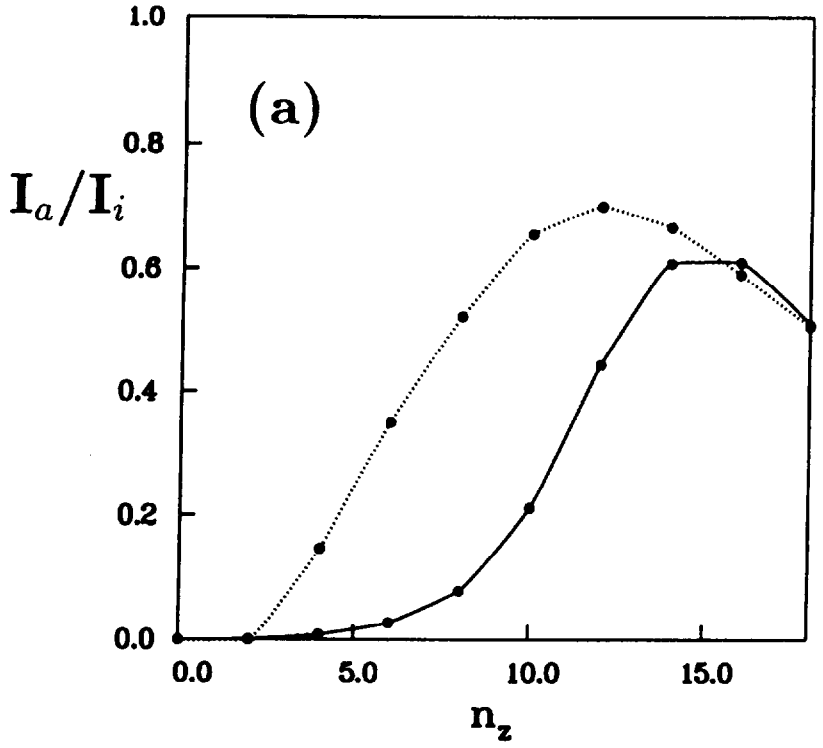

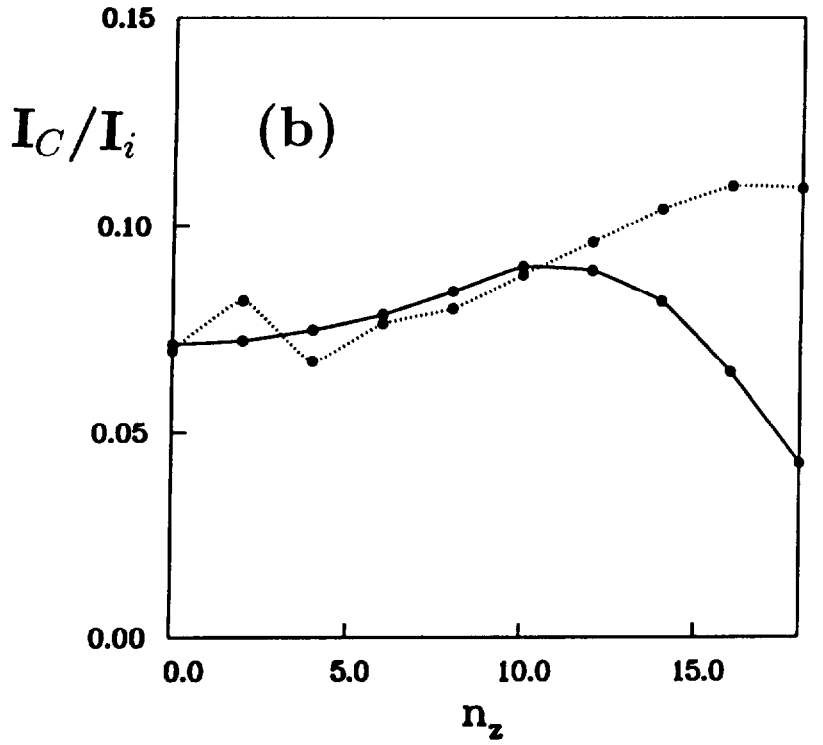

Fig. 13 a) the absorbed power; b; the converted power, and c) the transmitted power as a function of n_z for a T(D) scheme with $\nu_D = 0.5$ (solid) and 0.2 (dotted). The beryllium concentration is 0.05. The deuterium cyclotron resonance is not included in the calculation region.

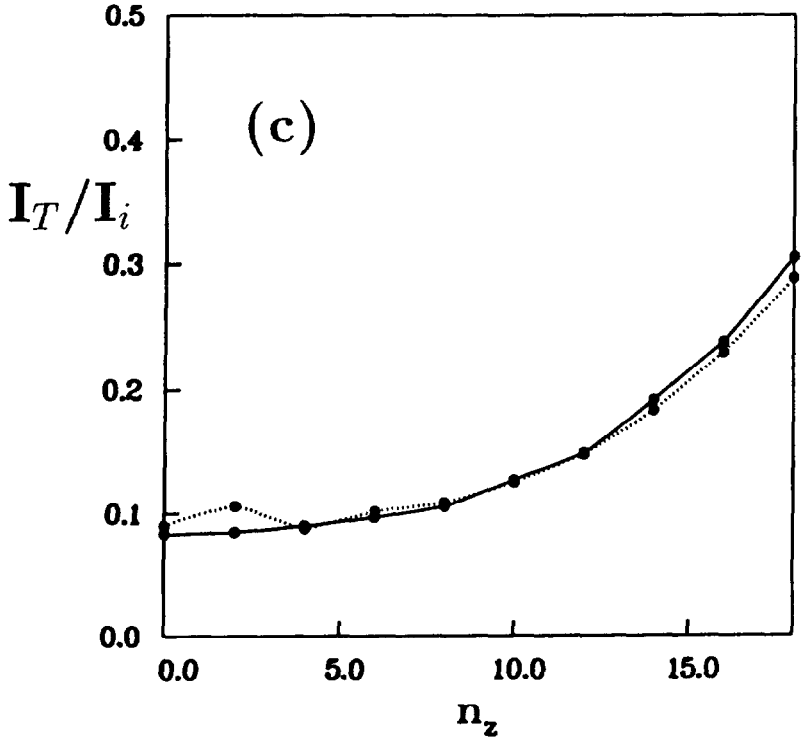
(c)
I_T/I_i
0.5
0.4
0.3
0.2
0.1
0.0
0.0
5.0
10.0
15.0
n_z

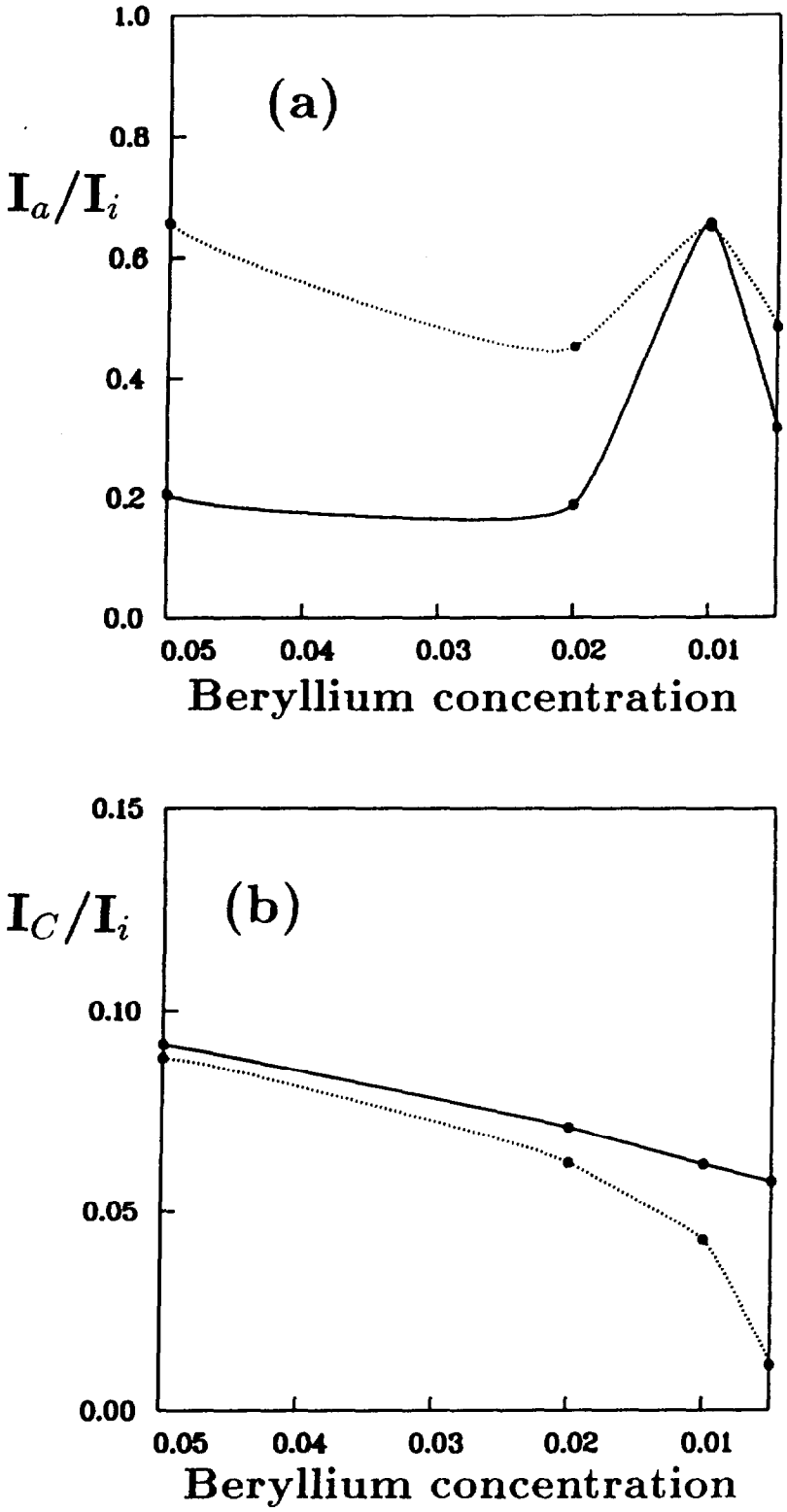

Fig. 14 a) the absorbed power: b) the converted power, and c) the transmitted power as a function of the beryllium concentration for a T(D) scheme with $\nu_D = 0.5$ (solid) and 0.2 (dotted). $n_z = 10$. The deuterium cyclotron resonance is not included in the calculation region.

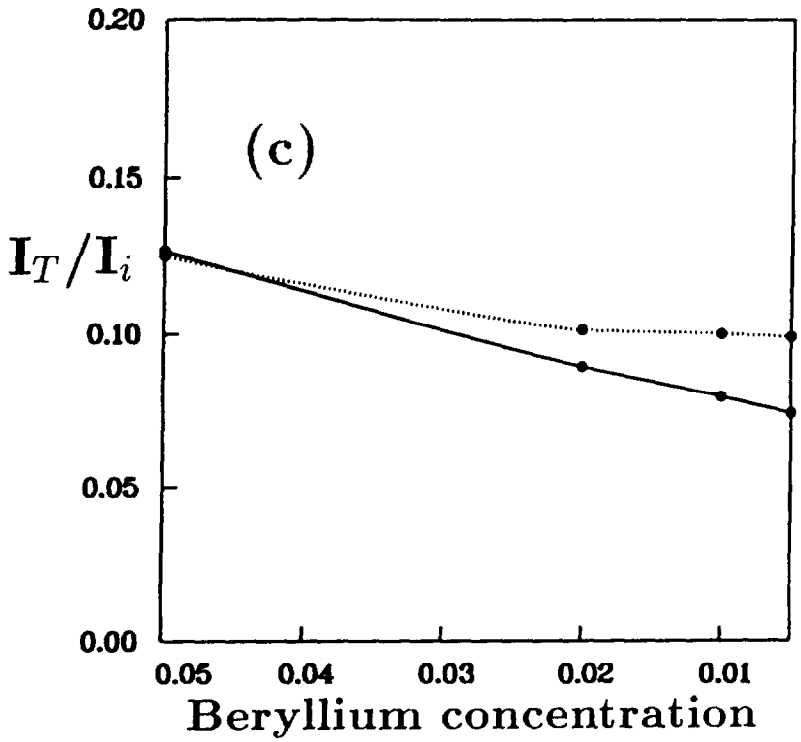
0.20
0.15
0.10
0.05
0.00
(c)
I_T/I_i
0.05
0.04
0.03
0.02
0.01
Beryllium concentration

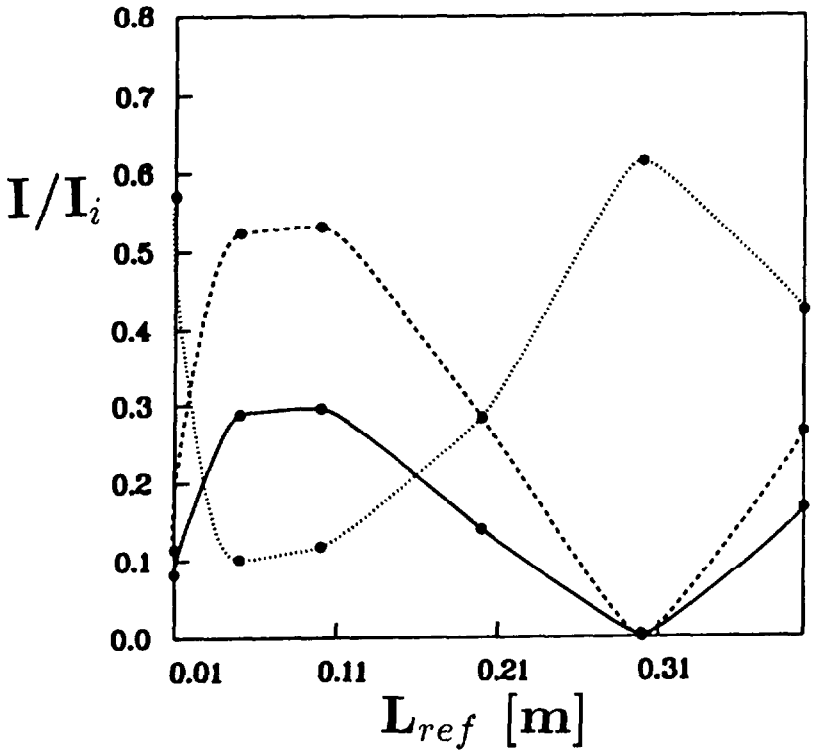

Fig. 15 The converted power (solid), the reflected (dotted) and the local estimate for the conversion (Eq.(24); dashed) for a case where we assume a complete reflection of the fast wave from a wall situated at a distance L_{ref} from the right end of the plasma slab. A D(^{3}He) case with $n_z = 6$ and $\nu_{^3He} = 0.028$.

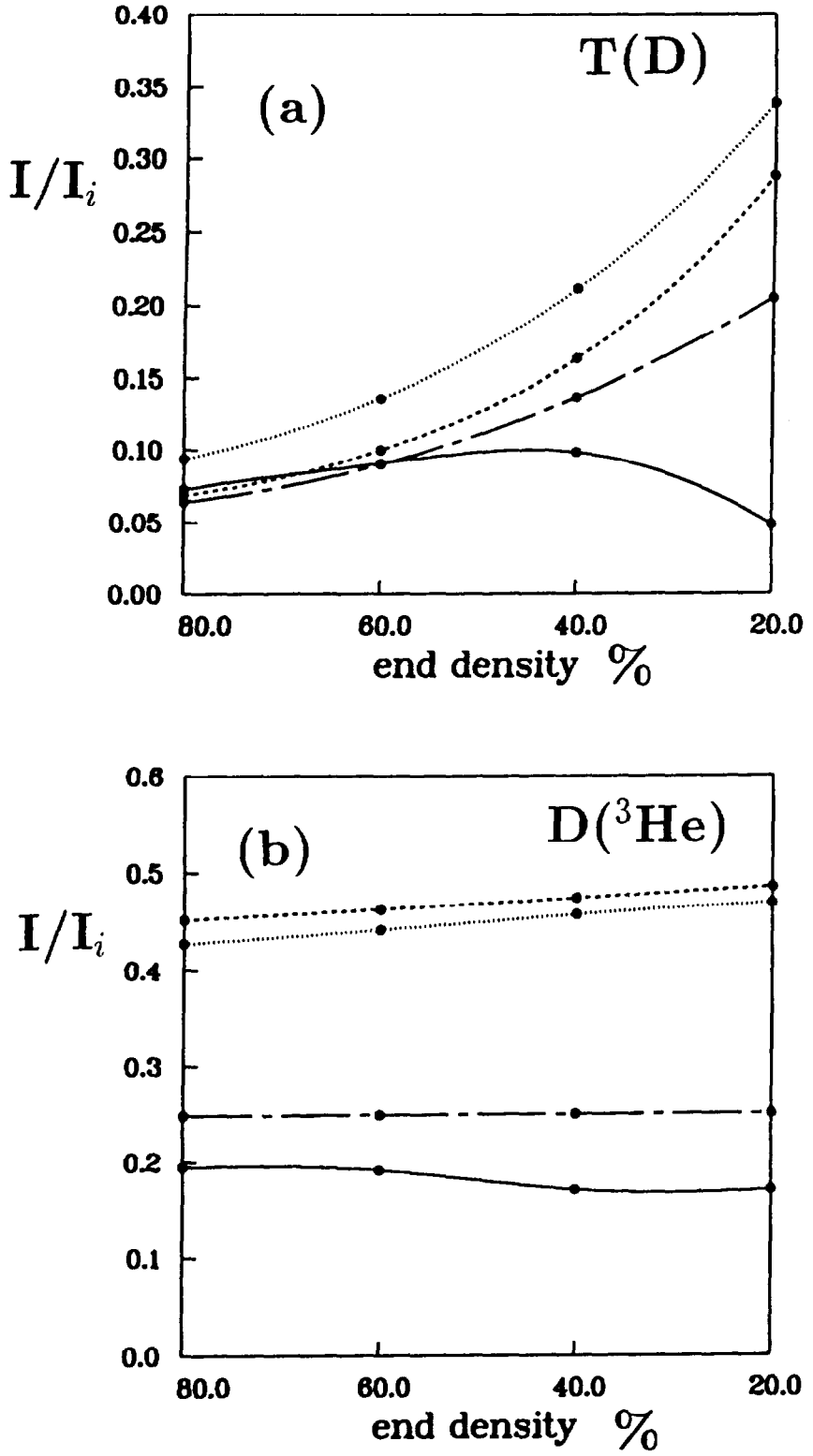

Fig. 16 The converted power (solid), the transmitted power (dotted), and the corresponding Budden estimates (chain dashed and dashed, respectively) as functions of the right end density (in per cent of the left end density) with a linear density gradient. a) the D(T) scheme with $\nu_D = 0.5$ and $n_z = 10$; b) the D(^{3}He) scheme with $\nu_{^3He} = 0.045$ and $n_z = 6$; c) the D(H) scheme with $\nu_H = 0.05$ and $n_z = 6$.

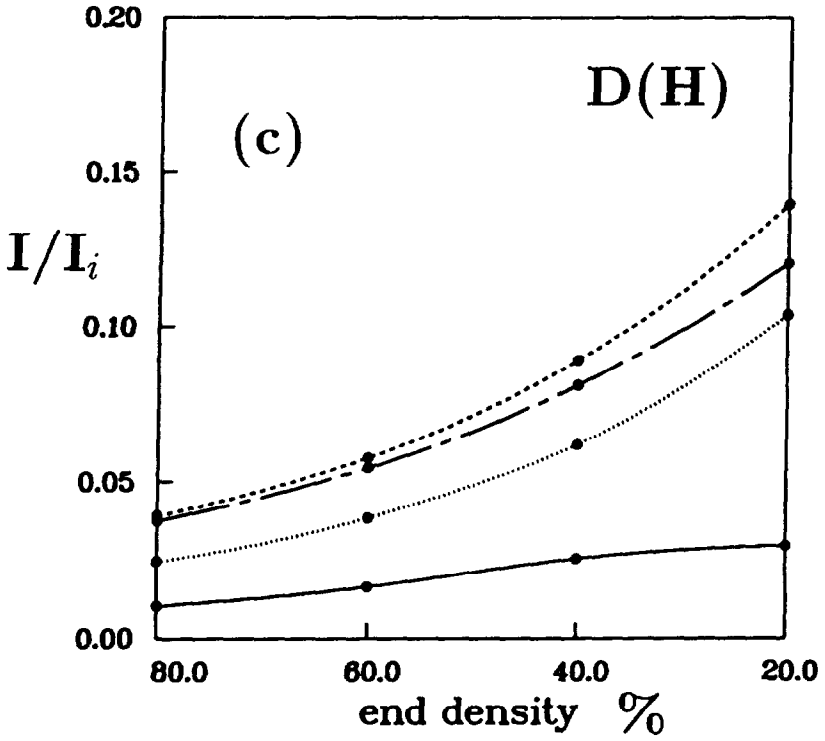
0.20
0.15
0.10
0.05
0.00
I/I_i
(c)
D(H)
80.0
60.0
40.0
20.0
end density %

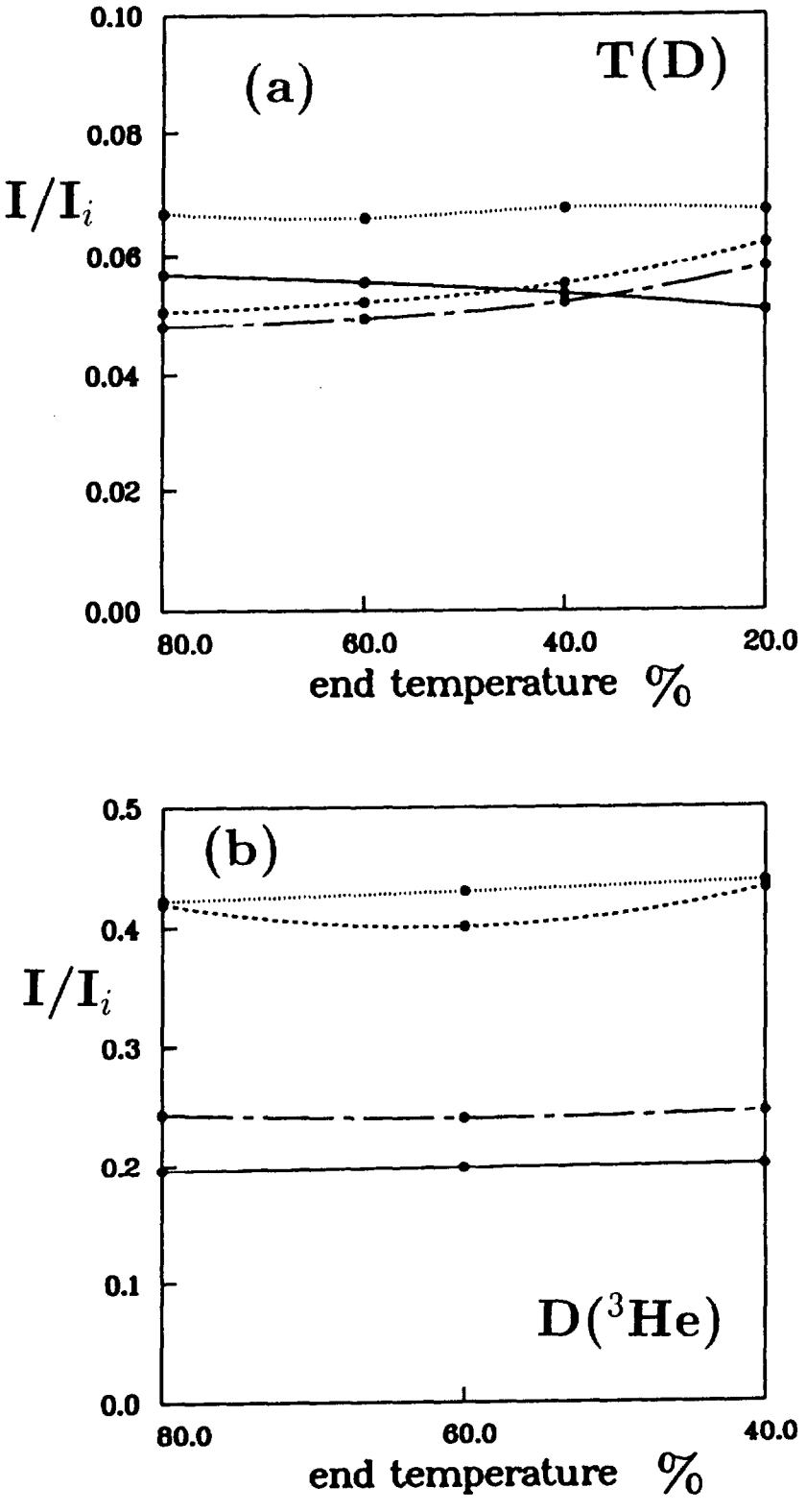

Fig. 17 The converted power (solid), the transmitted power (dotted), and the corresponding Budden estimates (chain dashed and dashed) as functions of the right end temperature (in per cent of the left end temperature) with a linear temperature gradient. a) the D(T) scheme with $\nu_D = 0.5$ and $n_z = 10$; b) the D(^{3}He) scheme with $\nu_{^3He} = 0.045$ and $n_z = 6$; c) the D(H) scheme with $\nu_H = 0.05$ and $n_z = 6$.

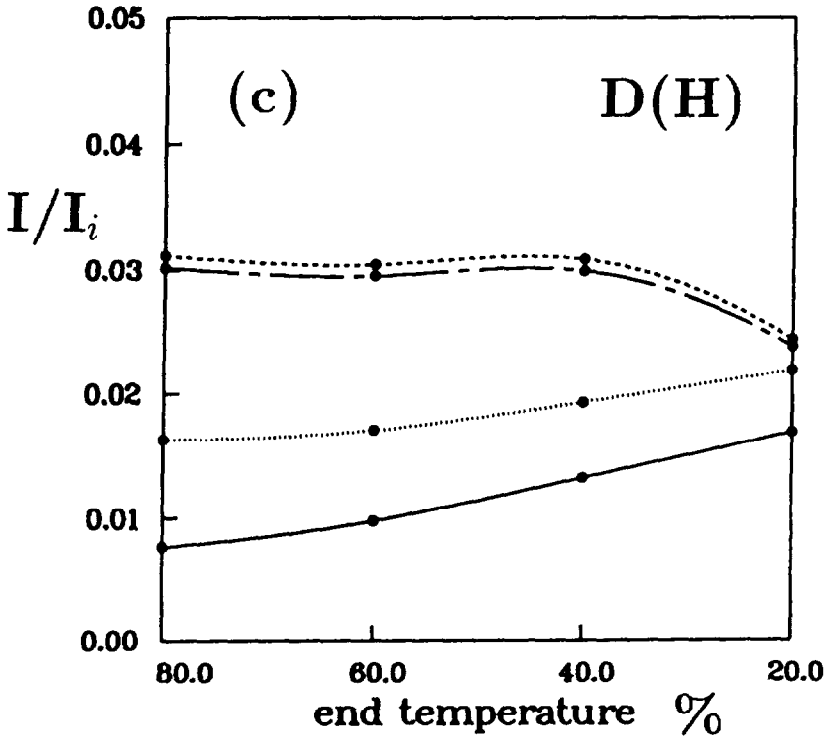
0.05
0.04
0.03
0.02
0.01
0.00
(c)
D(H)
I/I_i
80.0
60.0
40.0
20.0
end temperature %

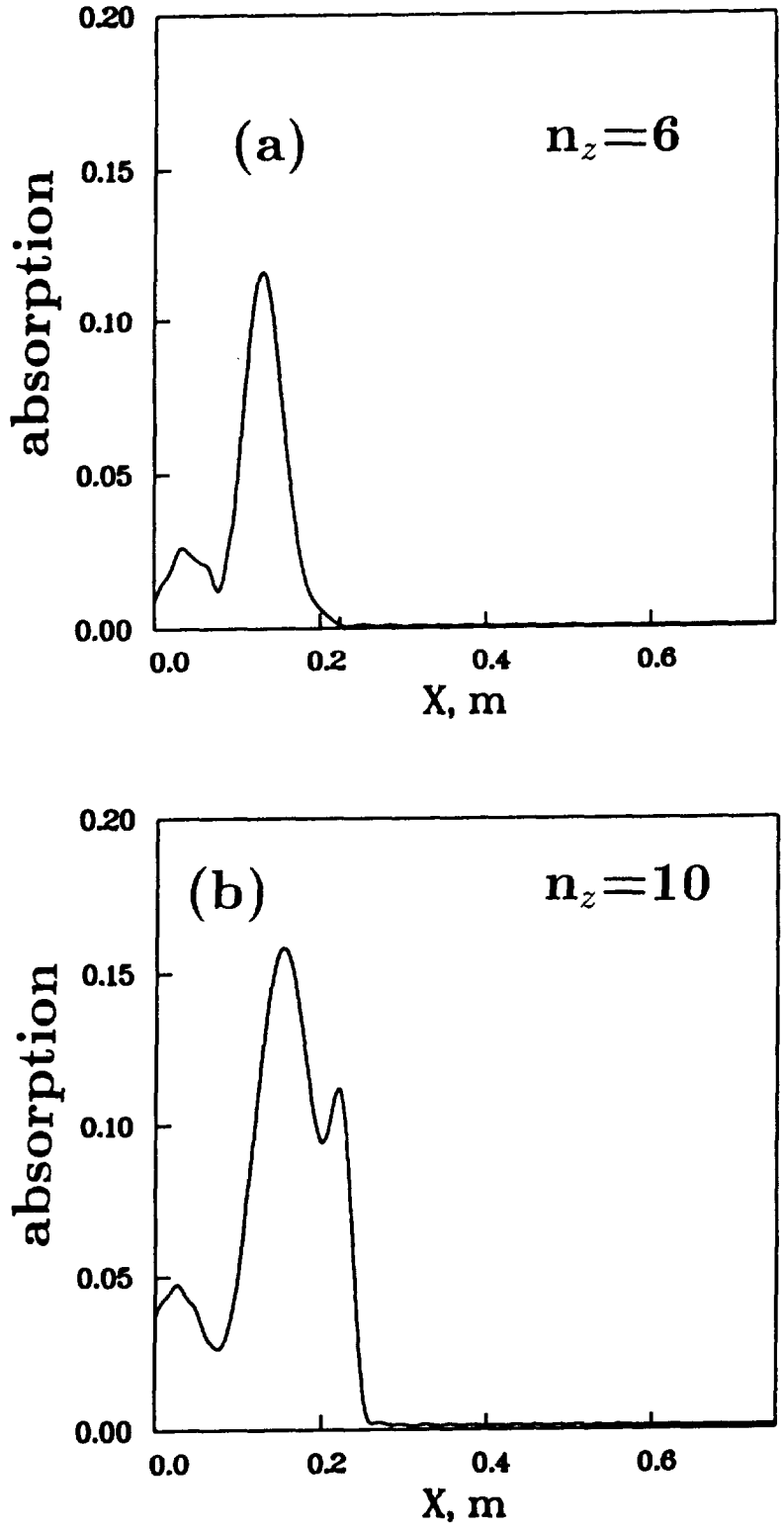

Fig. 18 The power absorption profile (in arbitrary units) for a T(D) case with $\nu_D = 0.1$. The cyclotron resonance is located at approximately $x = 0.1$ m and the mode conversion point at $x = 0.23$ m. a) $n_z = 6$, b) $n_z = 10$.

Appendix I

THE JET TEAM

JET Joint Undertaking, Abingdon, Oxon, OX14 3EA, U.K.

J.M. Adams[1], H. Altmann, A. Andersen[14], P. Andrew[18], M. Angelone[29], S.A. Arshad, W. Bailey, P. Ballantyne, B. Balet, P. Barabaschi, R. Barnsley[2], M. Baronian, D.V. Bartlett, A.C. Bell, I. Benfatto[5], G. Benali, H. Bergsaker[11], P. Bertoldi, E. Bertolini, V. Bhatnagar, A.J. Bickley, H. Bindslev[14], T. Bonicelli, S.J. Booth, G. Bosia, M. Botman, D. Boucher, P. Boucquey, P. Breger, H. Brelen, H. Brinkschulte, T. Brown, M. Brusati, T. Budd, M. Bures, T. Businaro, P. Butcher, H. Buttgereit, C. Caldwell-Nichols, D.J. Campbell, P. Card, G. Celentano, C.D. Challis, A.V.Chankin[23], D. Chiron, J. Christiansen, C. Christodoulopoulos, P. Chuilon, R. Claesen, S. Clement, E. Clipsham, J.P. Coad, M. Comiskey[4], S. Conroy, M. Cooke, S. Cooper, J.G. Cordey, W. Core, G. Corrigan, S. Corti, A.E. Costley, G. Cottrell, M. Cox[7], P. Cripwell, H. de Blank[15], H. de Esch, L. de Kock, E. Deksnis, G.B. Denne-Hinnov, G. Deschamps, K.J. Dietz, S.L. Dmitrenko, J. Dobbing, N. Dolgetta, S.E. Dorling, P.G. Doyle, D.F. Düchs, H. Duquenoy, A. Edwards, J. Ehrenberg, A. Ekedahl, T. Elevant[11], S.K. Erents[7], L.G. Eriksson, H. Fajemirokun[12], H. Falter, D. Flory, J. Freiling[15], C. Froger, P. Froissard, K. Fullard, M. Gadeberg, A. Galetsas, D. Gambier, M. Garribba, P. Gaze, R. Giannella, A. Gibson, R.D. Gill, A. Girard, A. Gondhalekar, C. Gormezano, N.A. Gottardi, C. Gowers, B.J. Green, R. Haange, G Haas, A. Haigh, G. Hammett[6], C.J. Hancock, P.J. Harbour, N.C. Hawkes[7], P. Haynes[7], J.L. Hemmerich, T. Hender[7], F.B. Herzog, R.F. Herzog, J. Hoekzema, J. How, M. Huart, L Hughes, T.P. Hughes[4], M. Hugon, M. Huguet, A. Hwang[7], B. Ingram, M. Irving, J. Jacquinot, H. Jaeckel, J.F. Jaeger, G. Janeschitz[13], S. Jankowicz[22], O.N. Jarvis, F. Jensen, E.M. Jones, L.P.D.F. Jones, T.T.C. Jones, J-F. Junger, E. Junique, A. Kaye, B.E. Keen, M. Keilhacker, G.J. Kelly, W. Kerner, R. Konig, A. Konstantellos, M. Kovanen[20], G. Kramer[15], P. Kupschus, R. Lässer, J.R. Last, B. Laundy, L. Lauro-Taroni, K. Lawson[7], M. Lennholm, A. Loarte, R. Lobel, P. Lomas, M. Loughlin, C. Lowry, B. Macklin, G. Maddison[7], G. Magyar, W. Mandl[13], V. Marchese, F. Marcus, J. Mart, E. Martin, R. Martin-Solis[8], P. Massmann, G. McCracken[7], P. Meriguet, P. Miele, S.F. Mills, P. Millward, R. Mohanti[17], P.L. Mondino, A. Montvai[3], S. Moriyama[28], P. Morgan, H. Morsi, G. Murphy, M. Mynarends, R. Myrnäs[16], C. Nardone, F. Nave[21], G. Newbert, M. Newman, P. Nielsen, P. Noll, W. Obert, D. O'Brien, J. O'Rourke, R. Ostrom, M. Ottaviani, M. Pain, F. Paoletti, S. Papastergiou, D. Pasini, A. Peacock, N. Peacock[7], D. Pearson[12], R. Pepe de Silva, G. Perinic, C. Perry, M. Pick, R. Pitts[7], J. Plancoulaine, J-P. Poffé, F. Porcelli, L. Porte[19], R. Prentice, S. Puppin, S. Putvinsko[23], G. Radford[9], T. Raimondi, M.C. Ramos de Andrade, P-H. Rebut, R. Reichle, E. Righi, F. Rimini, D. Robinson[7], A. Rolfe, R.T. Ross, L. Rossi, R. Russ, P. Rutter, H.C. Sack, G. Sadler, G. Saibene, J.L. Salanave, G. Sanazzaro, A. Santagiustina, R. Sartori, C. Sborchia, P. Schild, M. Schmid, G. Schmidt[6], B. Schunke, S.M. Scott, A. Sibley, R. Simonini, A.C.C. Sips, P. Smeulders, R. Stankiewicz[27], M. Stamp, P. Stangeby[18], D.F. Start, C.A. Steed, D. Stork, P.E. Stott, T.E. Stringer, P. Stubberfield, D. Summers, H. Summers[19], L. Svensson, J.A. Tagle[21], A. Tanga, A. Taroni, A. Tesini, P.R. Thomas, E. Thompson, K. Thomsen, J.M. Todd, P. Trevalion, B. Tubbing, F. Tibone, E. Usselmann, H. van der Beken, G. Vlases, M. von Hellermann, T. Wade, C. Walker, R. Walton[6], D. Ward, M.L. Watkins, M.J. Watson, S. Weber[10], J. Wesson, T.J. Wijnands, J. Wilks, D. Wilson, T. Winkel, R. Wolf, B. Wolle[24], D. Wong, C. Woodward, Y. Wu[25], M. Wykes, I.D. Young, L. Zannelli, Y. Zhu[26], W. Zwingmann.

PERMANENT ADDRESSES

1. UKAEA, Harwell, Didcot, Oxon, UK.
2. University of Leicester, Leicester, UK.
3. Central Research Institute for Physics, Academy of Sciences, Budapest, Hungary.
4. University of Essex, Colchester, UK.
5. ENEA-CNR, Padova, Italy.
6. Princeton Plasma Physics Laboratory, New Jersey, USA.
7. UKAEA Culham Laboratory, Abingdon, Oxon, UK.
8. Universidad Complutense de Madrid, Spain.
9. Institute of Mathematics, University of Oxford, UK.
10. Freien Universität, Berlin, F.R.G.
11. Swedish Energy Research Commission, S-10072 Stockholm, Sweden.
12. Imperial College of Science and Technology, University of London, UK.
13. Max Planck Institut für Plasmaphysik, Garching bei München, FRG.
14. Risø National Laboratory, Denmark.
15. FOM Instituut voor Plasmafysica, 3430 Be Nieuwegein, The Netherlands.
16. University of Lund, Sweden.
17. North Carolina State University, Raleigh, NC, USA
18. Institute for Aerospace Studies, University of Toronto, Downsview, Ontario, Canada.
19. University of Strathclyde, 107 Rottenrow, Glasgow, UK.
20. Nuclear Engineering Laboratory, Lapeenranta University, Finland.
21. CIEMAT, Madrid, Spain.
22. Institute for Nuclear Studies, Otwock-Swierk, Poland.
23. Kurchatov Institute of Atomic Energy, Moscow, USSR
24. University of Heidelberg, Heidelberg, FRG.
25. Institute for Mechanics, Academia Sinica, Beijing, P.R. China.
26. Southwestern University of Physics, Leshan, P.R. China.
27. RCC Cyfronet, Otwock Swierk, Poland.
28. JAERI, Naka Fusion Research Establishment, Ibaraki, Japan.
29. ENEA, Frascati, Italy.

At 1st June 1991